



HAL
open science

**RECONSTRUCTING EARLIEST DIAGENESIS
CONDITION USING SEDIMENTO LOGICAL AND
GEOCHEMICAL CHARACTERISTICS OF
GLAUCONITES . APPLICATION TO
LIMESTONEMARLSTONE ALTERNATION IN THE
BOULONNAIS**

Nicolas Tribovillard, Viviane Bout-Roumazeilles

► **To cite this version:**

Nicolas Tribovillard, Viviane Bout-Roumazeilles. RECONSTRUCTING EARLIEST DIAGENESIS CONDITION USING SEDIMENTO LOGICAL AND GEOCHEMICAL CHARACTERISTICS OF GLAUCONITES . APPLICATION TO LIMESTONEMARLSTONE ALTERNATION IN THE BOULONNAIS. *Annales de la Société Géologique du Nord*, 2025, 32, 10.54563/asgn.2568 . hal-04933152

HAL Id: hal-04933152

<https://hal.science/hal-04933152v1>

Submitted on 13 Feb 2025

HAL is a multi-disciplinary open access archive for the deposit and dissemination of scientific research documents, whether they are published or not. The documents may come from teaching and research institutions in France or abroad, or from public or private research centers.

L'archive ouverte pluridisciplinaire **HAL**, est destinée au dépôt et à la diffusion de documents scientifiques de niveau recherche, publiés ou non, émanant des établissements d'enseignement et de recherche français ou étrangers, des laboratoires publics ou privés.

RECONSTRUCTING EARLIEST DIAGENESIS CONDITION USING SEDIMENTO-LOGICAL AND GEOCHEMICAL CHARACTERISTICS OF GLAUCONITES. APPLICATION TO LIMESTONE-MARLSTONE ALTERNATION IN THE BOULONNAIS

Reconstitution des conditions de diagenèse très précoce à partir des caractéristiques sédimentologiques et géochimiques de glauconites — application à l'alternance calcaire-marne dans le Boulonnais

Nicolas Tribovillard

Université de Lille, UMR 8187 LOG – Laboratoire d'Océanologie et de Géosciences, CNRS, Univ. Littoral Côte d'Opale, IRD, 59000 Lille, France
nicolas.tribovillard@univ-lille.fr

Viviane Bout-Roumazeilles

Université de Lille, UMR 8187 LOG – Laboratoire d'Océanologie et de Géosciences, CNRS, Univ. Littoral Côte d'Opale, IRD, 59000 Lille, France

Résumé

Some of the geological formations of Upper Jurassic and Cretaceous age in the Boulonnais area (Strait of Pas-de-Calais, English Channel) show levels relatively rich in glauconite (a few weight% to 44 wt%). Recent works have shown that glauconite could have formed during (very) early diagenesis; this authigenic phyllosilicate could have thus witnessed the chemical conditions prevailing at the sediment-water interface or a short distance below it. This can be of particular interest in the case of the Assises de Croÿ Formation showing alternating carbonate beds and marly beds. The beds are of early diagenetic origin and contain populations of glauconite grains which formed even earlier. Glauconite can therefore be considered here as the privileged proxy to the sediment-water interface conditions during the development of the limestone-marl alternation, which is a common pattern in the sedimentary record worldwide. Glauconite was observed from the perspective of its chemical composition (including REE) as well as that of the particle size distribution. The results show that, if redox-proxying trace elements such as V, As, Ge can reflect the redox status of the conditions in which glauconite was formed, this is not the case for REE. The only parameter linked to REE which provides paleoenvironmental indications here is Σ REE, being negatively correlated with the sedimentation rate. It is suggested that REE were all the more incorporated to glauconite when the sedimentation rate was low, but without any appreciable fractionation among REE. Concerning the limestone/marl alternation, our results show that its development is linked neither to variations in redox conditions nor to hydrodynamic changes of the depositional environment. This is a diagenetic phenomenon, the cause of which remains to be determined. Finally, a relationship could be highlighted between the sedimentation rate and the size of the glauconite grains grown *in situ*.

Abstract

Les formations géologiques du Jurassique supérieur et du Crétacé du Boulonnais (détroit du Pas-de-Calais) peuvent présenter des teneurs notables en grain de glauconite (de quelques % pondéraux à 44 %). Des travaux récents ont montré que cette glauconite s'est formée au cours de la diagenèse (très) précoce; ce phyllosilicate authigénique aurait ainsi pu être le témoin des conditions paléo-environnementales — en particulier, chimiques — régnant à l'interface eau-sédiment ou à une courte distance au-dessous. Ceci peut être particulièrement intéressant dans le cas des Assises de Croÿ présentant une alternance de bancs carbonatés et d'interbancs marneux. Les bancs carbonatés sont d'origine diagénétique précoce et contiennent des populations de grains de glauconite qui se sont formés encore plus tôt. La glauconite peut donc être considérée ici comme l'indicateur privilégié des conditions d'interface eau-sédiment lors du développement de l'alternance calcaire-marne, qui est un faciès commun dans les archives sédimentaires mondiales. La glauconite a été observée du point de vue de sa composition chimique (y compris les Terres Rares) ainsi que de celui de la distribution de la taille des particules. Les résultats montrent que, si des éléments-traces tels que V, As, Ge peuvent refléter le statut redox des conditions dans lesquelles la glauconite s'est formée, ce n'est pas le cas pour les Terres Rares. Le seul paramètre lié aux Terres Rares qui fournisse ici des indications paléo-environnementales est Σ REE, qui est manifestement lié à la vitesse de sédimentation. Il est suggéré que les Terres Rares étaient d'autant plus incorporées à la glauconite que le taux de sédimentation était faible, mais sans fractionnement visible au sein des Terres Rares elles-mêmes. Par ailleurs, concernant les alternances, nos résultats montrent que leur évolution n'est liée ni aux variations des conditions redox ni à celles de l'hydrodynamique du milieu de dépôt. Il s'agit d'un phénomène principalement diagénétique dont la cause reste à déterminer (la condensation sédimentaire est une cause probable; J.-F. Deconinck, communication personnelle, 2024). Enfin, une relation a pu être mise en évidence entre la vitesse de sédimentation et la taille des grains de glauconite développés *in situ* : une relative condensation sédimentaire accompagne une augmentation de la taille des grains de glauconite. Au total, les grains de glauconite peuvent avoir une vraie valeur d'indicateur paléo-environnemental, à condition que leurs conditions de formation aient été bien définies.

1. INTRODUCTION

Glaucinite belongs to the family of authigenic green clay minerals often grouped under the name glaucony. It is a phyllosilicate close to illite, rich in iron (Fe) and potassium (K; Odin & Matter, 1981; Velde, 2014; Banerjee et al., 2012a, 2012b, 2016a, 2016b; Huggett et al., 2017; Huggett 2021; Bansal et al., 2020, 2022; Roy Choudhury et al. 2021a, 2021b). The work of Odin & Matter (1981) established a link between the chemical composition of glauconite and the duration of its formation during authigenesis. A K_2O content $> 8\%$ and a Fe_2O_3 content in the range of 24% - 28% would indicate growth lasting between 3.10^5 years and 1.10^6 y. These works, often taken up by other authors, have been questioned (e.g., Chafetz & Reid, 2000; El Albani et al., 2005; Baldermann et al., 2013, 2022; Föllmi, 2016; Meunier & El Albani, 2007; Wilmsen & Bansal, 2021) and Tribovillard et al. (2023a) showed that, in some cases, glauconite minerals corresponding to the “highly evolved” stage defined by Odin & Matter (1981) were nevertheless formed during (very) early diagenesis. The present study does not address the issue of exact time requirement for formation of glauconite. See for instance the relation between K_2O concentrations and the age of glauconite in the Gulf of Guinea (Odin, 1988; Tallobre et al., 2019; Giresse, 2022 and references therein). The focus is here set on the relative chronology. For instance, early (or earliest diagenesis) means that the phenomenon occurred while life in-fauna was dwelling the sediment. It is not discussed how long such dwelling lasted (years or thousands of years?); only the successive steps of the diagenetic course are taken into consideration. Regardless of how long it is grown, glauconite is an authigenic mineral and its chemical composition should reflect (at least partly) the conditions of diagenesis. If, in addition, this mineral can form during very early diagenesis, then it may reflect the paleo-environmental conditions prevailing at the sediment-water interface, or immediately below this interface. In other words, glauconite can be considered to be a marker of depositional conditions and subsequent diagenesis episodes. In this perspective, we studied glauconites of different ages (late Jurassic to Cretaceous) present in the Boulonnais area (northernmost France) with an emphasis set on trace elements and, in particular, Rare Earths Elements (REE). One of the aims of the present work is to assess the robustness of the chemical composition of glauconitic grains, used as a tool in paleoenvironmental reconstructions, which is of interest to the community of paleoenvironmentalists and sedimentary geochemists. In particular, we examined the limestone-marl alternations of the uppermost Jurassic (Assises de Croï Formation) to determine whether the carbonate beds vs. marly interbeds were generated under contrasting environmental conditions. Relatively few studies were devoted so far to the REE distribution in glauconites (e.g., Fleet et al., 1980; Stille & Clauer, 1994; Jarrar et al., 2000;

Wigley & Compton, 2007; Kechiched et al., 2018; Giresse et al., 2021) and this paper aims to decipher which information can be derived from this geochemical parameter.

2. MATERIAL, METHODS AND A REMINDER OF SOME PREVIOUS RESULTS

In the Boulonnais region, glauconite is commonly observed in the geological formations of the Upper Jurassic and Upper Cretaceous, cropping out between Boulogne-sur-mer and Cap Blanc-Nez, along the Strait of Pas-de-Calais (a.k.a. English Channel; Fig. 1), and some glauconite-rich levels or geological formations have been studied recently (Tribovillard et al., 2021, 2023a, 2023b). Studies on the glauconitic levels at the base of the Cenomanian chalk showed that this mineral was not reworked and had formed *in situ* thanks to episodes of decreased sedimentation rate in connection with the great transgression of the Late Cretaceous (Amorosi & Centineo, 2000; Tribovillard et al., 2021). By extending their study to the formations of the middle part of the Cretaceous (glauconitic sandstones of the Aptian-Albian and transition layers with the chalk) and those of the Upper Jurassic, Tribovillard et al. (2023a) concluded that the glauconite of the deposits studied had formed in shallow marine environments. Furthermore they showed that oyster patch reefs, frequent in the Jurassic of the Boulonnais, must have been an environment conducive to the synsedimentary formation of glauconite. This work also showed that the richness of glauconite in vanadium (V) and arsenic (As) could be directly linked to the redox conditions that prevailed during authigenesis. Finally, the work by Tribovillard et al. (2023b) focused on the glauconite present in great abundance in the limestone-marl alternations of the upper Tithonian Assises de Croï Formation (Fm). The limestone beds resulted from the coalescence of limestone nodules formed during early diagenesis. This study shows that the glauconite, trapped within the nodules and beds, was even earlier than the formation of the nodules, in the course of the diagenetic stages. Based on the three studies mentioned above, we intend to know: 1) whether the glauconites that formed in different environments and at different ages show a contrasting REE signature, and 2) whether the REE distribution of such an authigenic mineral could be a useful tool for paleo-environmental reconstructions, when examined in conjunction with redox-proxying trace metals.

The samples examined in the present study are those presented in the works mentioned above (Tribovillard et al., 2021, 2023a, 2023b; plus four samples of chalk: Craie1-4); their locations are indicated in Table 1. The analytical data used here (gathered in Table 2) come from these papers (samples ONM1-4 from Tribovillard et al., 2021; samples of the Assises de Croï Fm from Tribovillard et al., 2023b; the other samples from Tribovillard et al., 2023a). The REE data of the samples

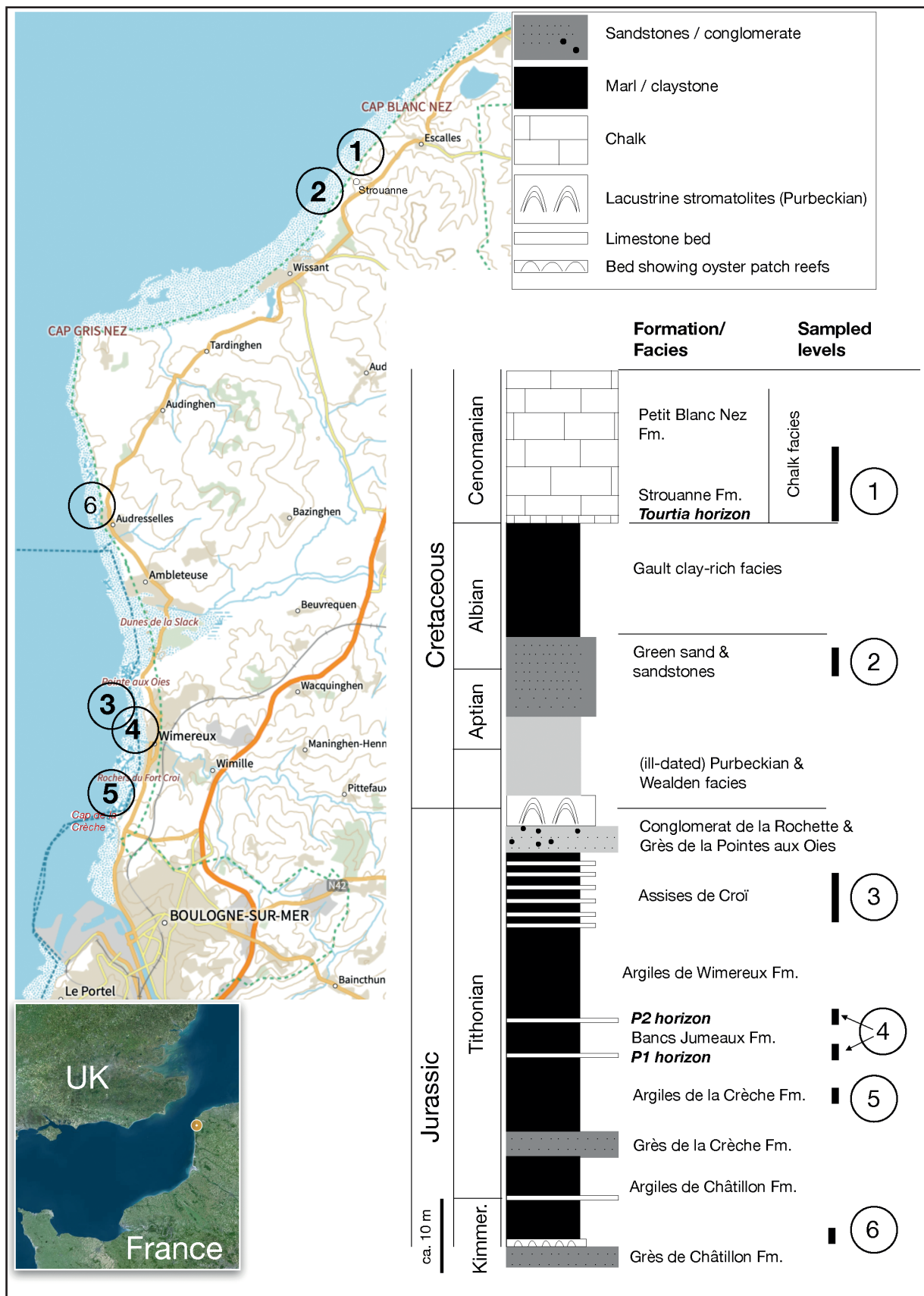


Fig. 1. Location and stratigraphy of the glauconite-rich levels studied here (numbered 1 to 6) along the shoreline of the Boulonnais region, also called Coast of Opal, in the Pas-de-Calais Strait (English Channel). Map drawn using Geoportail © IGN
 Fig. 1. Localisation et stratigraphie des niveaux riches en grains de glauconite étudiés ici (numérotés de 1 à 6) le long du littoral de la région boulonnaise, également appelée Côte d'Opale, dans le détroit du Pas-de-Calais. Carte réalisée à l'aide du Géoportail © IGN

Geological formations	Levels rich in glauconite in Boulonnais	Location (see Fig. 1)	# in Fig. 1	Samples
Cenomanian Chalk	Glauconious chalk at the lowermost part of the formation, beginning with the so-called Tourtia bed, rich in glauconite	Beach between Strouanne and Cap Blanc Nez	1	Craie 1 to 4; ONM1 to 4; T; Cenom
Aptian-Albian sandstones	Dark-colored sands and sandstones visible at low tide	Strouanne Beach	2	GC1; SP
Assise de Croï	Alternating carbonate levels and marly interbeds	Sampled at Pointe aux Oies (North Wimereux), pictured at Rochers du Fort Croï (South Wimereux)	3	Beds A to G; interbed A to G
Bancs Jumeaux	P1 & P2: phosphate- and clastic-rich carbonate levels, at the base and top of the formation	South to Pointe aux Oies (place called Pointe de la Rochette)	4	P1 & P2
Argiles de la Crèche	Silty marls at the very base of the formation	Rochers du Fort Croï (South Wimereux)	5	Not mentioned in this work
Argiles de Châtillon	Coquina beds at the Kimmeridgian-Tithonian boundary	North of Audresselles (Cran du Noirda)	6	Not mentioned in this work
Argiles de Châtillon	Oyster patch reefs at the base of the formation (the Boundary Bed, Kimmeridgian)	North of Audresselles (Cran du Noirda)	6	PR1 to PR4

Table 1. Stratigraphy, short description and location of the levels sampled for the present study. Sample names and locations refer to Fig. 1.

Tableau 1. Stratigraphie, brève description et localisation des niveaux échantillonnés pour la présente étude. Les noms et emplacements des échantillons font référence à la figure 1.

of the Assises de Croï Fm examined in the present study were unpublished yet (Table 2). All the samples analyzed but four are populations of glauconite grains extracted from the rocks as explained below. Four bulk-rock samples of glauconitic chalk were added to complement our understanding of the geochemistry of the glauconite of the chalk. These samples are labeled craie1 to craie4; they correspond to the four facies studied by Tribovillard et al. (2021).

The chemical analyzes were carried out by the SARM-CRPG facility of the CNRS in Nancy on glauconite grains extracted from the rocks. This glauconite was isolated at Lille University after acid treatment (HCl) and magnetic separation with an isodynamic Frantz apparatus, according to the protocol described in Tribovillard et al. (2023a). The chemical analyzes were carried out by ICP-OES and ICP-MS according to the protocols described in Carignan et al. (2004). REEs have been normalized using the Post-Archean Australian Shale or PAAS (Taylor & McLennan, 1985). The anomalies in cerium (Ce) and europium (Eu) were calculated according to Rollinson and Pease (2021) and the ratios La/LuN, La/SmN and Gd/YbN (the subscript N stands for normalized) were calculated to highlight possible enrichments in light, medium or heavy REE (Rollinson & Pease, 2021). As regards the determination of glauconite, phase identification, based on peak positions (d-spacing) and relative intensities, has been performed on X-ray Diffraction patterns via Rietveld refinement on disoriented powder (X'Pert high score Plus software – PDF4 database). This method was used in each of

our previous studies (Tribovillard et al., 2021, 2023a, 2023b). Lastly, in an attempt to observe the core of the glauconite grains or a possible zoning, handpicked grains of glauconite were embedded in resin and a thin section was cut for SEM imaging and photonic microscope observation.

Before exposing the results for the present study, some results mentioned in our previous papers cited above must be reminded here, complemented with new illustrations. Glauconite is the only green mineral identified in the Mesozoic rocks studied in the Boulonnais. All XRD analyses yielded the same diffractograms, exemplified in Fig. 2. Some previous observations performed on the grains may be summarized as follows. The glauconite grains show a homogeneous dark color, whatever formation they come from (Fig. 3). They usually show cracks, discrete or not (Fig. 4A-D; Tribovillard et al., 2023b). Last, high contents in iron, aluminum and potassium are the usual geochemical markers of highly evolved glauconite. See also the discussion herein below about the correlations between K_2O and Rb, and between Sm and Nd, also confirming the high maturity.



Samples	As	Ba	Be	Bi	Cd	Co	Cr	Cs	Cu	Ga	Ge	Hf	In	Mo	Nb	Ni	Pb	Rb	Sb	Sc	Sn	Sr	Ta	Th	U	V	W	Y	Zn	
	µg/g	µg/g	µg/g	µg/g	µg/g	µg/g	µg/g	µg/g	µg/g	µg/g	µg/g	µg/g	µg/g	µg/g	µg/g	µg/g	µg/g	µg/g	µg/g	µg/g	µg/g	µg/g	µg/g	µg/g	µg/g	µg/g	µg/g	µg/g	µg/g	µg/g
GG1	25,1	68,4	6,55	<	0,03	28,5	218	4,57	9,5	22,1	5,33	2,82	0,06	<L.D.	11,7	52,5	3,80	211	0,48	25,37	0,92	41,2	0,90	0,59	0,31	322	<L.D.	1,72	89,1	
PR1	26,9	13,6	6,30	0,12	0,03	9,95	138	0,86	4,3	12,8	8,15	1,34	0,05	<L.D.	2,77	18,0	5,60	279	0,21	11,32	0,38	23,5	0,09	0,17	0,13	131	<L.D.	0,62	72,0	
PR2	26,0	13,6	6,27	0,11	0,03	9,91	139	0,87	3,9	12,7	8,11	1,30	0,04	<L.D.	2,77	17,8	5,27	274	0,20	11,39	0,37	22,1	0,09	0,20	0,13	128	<L.D.	0,68	71,7	
PR3	26,1	63,9	7,03	0,07	0,02	29,5	267	5,00	23,0	23,3	5,31	3,18	0,07	0,65	19,4	60,2	45,5	216	0,57	24,83	1,16	44,7	1,40	1,34	0,68	327	<L.D.	3,30	99,0	
PR4	26,9	16,3	7,17	0,45	<L.D.	9,97	143	0,93	11,5	12,9	8,03	1,36	0,05	<L.D.	2,76	21,1	9,39	279	0,31	11,58	0,51	22,2	0,10	0,25	0,27	130	<L.D.	0,78	70,9	
P1	28,4	44,3	8,29	0,08	0,03	14,7	302	2,18	13,1	22,2	8,08	2,51	0,05	0,65	5,84	22,8	9,89	235	0,50	14,96	1,44	33,0	0,35	2,10	0,85	150	<L.D.	10,9	74,9	
P2	27,2	47,6	5,92	0,13	0,04	12,1	280	1,70	11,6	16,0	8,57	3,14	0,04	<L.D.	6,35	17,7	4,63	205	0,30	13,45	0,91	38,1	0,37	1,95	0,46	138	<L.D.	6,51	71,8	
T	5,55	11,9	5,90	0,08	<L.D.	25,3	110	9,36	<	12,8	4,73	1,52	0,04	<L.D.	2,45	49,4	3,72	242	0,47	9,71	0,76	18,1	0,18	0,22	0,10	86,8	<L.D.	0,73	46,8	
SP	5,83	488	5,84	0,09	0,04	25,0	118	7,28	<	12,7	4,97	1,40	0,05	<L.D.	2,47	46,7	2,39	251	0,45	10,08	0,78	25,0	0,19	0,15	0,13	90,5	<L.D.	0,61	51,6	
Cenom	5,87	15,0	5,86	0,09	0,02	25,9	115	8,51	3,6	13,5	4,98	1,32	0,04	<L.D.	2,63	53,1	2,27	257	0,53	9,86	0,86	25,9	0,18	0,30	0,15	96,2	<L.D.	0,57	55,5	
Craie 1	4,25	110	1,52	0,12	0,06	12,6	39,6	3,03	4,7	5,90	1,47	1,01	<L.D.	<L.D.	3,09	29,8	4,95	71	0,36	4,19	0,78	491,9	0,25	2,43	1,25	37,8	<L.D.	10,19	27,3	
Craie 2	3,70	52,3	1,43	0,15	0,04	10,9	36,2	2,80	4,1	5,45	1,28	0,96	<L.D.	<L.D.	2,95	25,3	3,99	67	0,29	4,07	0,87	437,9	0,25	2,16	1,04	35,3	<L.D.	8,92	21,7	
Craie 3	3,82	72,2	1,40	0,17	0,05	9,14	38,7	2,86	6,0	6,24	1,35	1,26	<L.D.	<L.D.	3,74	24,8	5,30	65	0,34	4,72	0,98	526,9	0,32	2,93	1,15	39,0	<L.D.	11,25	26,2	
Craie 4	11,5	87,3	3,79	0,15	0,07	24,0	76,9	6,46	6,5	10,2	3,15	1,68	0,03	<L.D.	4,24	53,7	7,88	155	0,51	7,75	1,03	321,3	0,34	3,28	2,48	70,7	<L.D.	13,03	39,4	
ONM 1	5,86	19,4	6,15	0,09	<L.D.	24,3	115	9,24	48,8	13,1	4,80	1,34	0,04	<L.D.	2,83	53,0	2,39	252	0,60	9,32	2,93	32,8	0,18	0,17	0,13	92,0	<L.D.	0,39	54,9	
ONM 2	6,08	34,4	5,68	0,10	<L.D.	33,3	109	9,14	28,8	13,9	4,75	1,19	0,03	<L.D.	3,18	64,6	2,04	258	0,76	8,15	2,86	25,0	0,17	0,09	0,09	92,4	<L.D.	0,26	50,0	
ONM 3	5,82	48,3	5,82	0,10	<L.D.	29,2	113	8,46	34,2	14,5	5,25	1,72	<L.D.	<L.D.	3,13	68,8	2,04	249	0,76	7,83	1,79	24,0	0,15	0,10	0,10	94,5	<L.D.	0,29	58,2	
ONM 4	6,09	31,0	6,63	0,10	<L.D.	25,4	125	9,61	5,4	13,4	5,07	1,30	0,05	<L.D.	2,66	52,6	2,81	262	0,53	9,84	1,01	28,1	0,18	0,15	0,15	95,8	<L.D.	0,47	54,3	
Bed A	30,3	14,6	8,14	0,09	0,03	11,8	260	0,81	9,6	18,2	8,51	1,81	0,04	<L.D.	3,71	21,0	4,04	279	0,19	15,42	0,62	20,1	0,14	0,73	0,27	146	<L.D.	3,47	93,9	
Bed B	31,5	21,1	7,44	0,11	0,03	9,64	165	0,79	8,5	16,8	8,07	1,79	0,04	<L.D.	2,89	17,9	5,99	270	0,16	13,17	0,81	19,8	0,13	0,56	0,23	131	<L.D.	0,93	85,4	
Bed C	31,0	14,9	7,44	0,12	0,02	9,34	173	0,73	7,4	15,5	8,19	1,81	0,05	<L.D.	2,81	17,2	5,21	279	0,16	12,84	0,69	19,5	0,11	0,33	0,22	136	<L.D.	0,88	83,2	
Bed D	32,6	18,2	8,02	0,10	0,03	8,53	207	0,88	9,6	17,5	8,47	2,42	0,05	<L.D.	3,97	17,8	5,08	272	0,17	14,11	1,19	21,0	0,18	0,68	0,39	158	<L.D.	2,28	85,8	
Bed E	29,3	18,4	7,68	0,13	0,07	10,5	200	1,09	7,3	15,7	8,18	1,75	0,05	<L.D.	3,95	18,6	6,07	290	0,20	12,13	0,65	20,7	0,21	1,84	0,43	136	<L.D.	5,01	86,7	
Bed F	25,3	25,1	8,74	0,10	0,02	11,9	241	1,64	9,8	19,4	7,87	2,50	0,05	<L.D.	4,97	18,2	5,21	259	0,16	14,17	0,97	23,7	0,38	0,79	0,38	144	<L.D.	5,51	91,9	
Bed G	26,3	30,8	8,99	0,10	0,04	12,7	485	1,78	24,2	21,7	6,88	3,17	0,05	0,55	7,64	21,8	9,06	239	0,27	16,75	1,33	32,6	0,59	2,35	0,82	174	<L.D.	20,9	127	
InterBed A	29,8	20,1	8,36	0,09	0,03	11,8	238	1,08	8,5	18,2	8,40	2,32	0,04	<L.D.	3,53	19,1	4,33	273	0,19	16,19	0,94	18,6	0,16	1,23	0,32	146	<L.D.	4,98	89,5	
InterBed B	34,3	16,7	8,05	0,10	<L.D.	9,87	178	0,73	7,3	17,8	8,42	2,23	0,04	<L.D.	3,06	17,8	5,10	273	0,21	14,54	0,93	17,0	0,14	0,89	0,26	137	<L.D.	3,21	82,2	
InterBed C	31,0	14,8	7,89	0,12	<L.D.	9,59	178	0,78	4,5	16,2	8,00	2,04	0,04	<L.D.	2,82	17,3	5,35	281	0,17	13,32	0,81	18,2	0,12	0,56	0,24	143	<L.D.	2,04	76,4	
InterBed D	32,4	16,1	7,66	0,10	0,02	7,09	191	0,78	5,0	16,1	7,97	2,19	0,05	1,31	3,55	15,3	4,98	272	0,19	13,60	0,77	18,3	0,15	0,81	0,33	150	<L.D.	2,67	70,2	
InterBed E	29,0	16,6	7,13	0,11	0,02	10,0	187	0,93	6,1	14,8	8,23	1,98	0,04	0,62	3,41	17,6	5,93	266	0,21	12,14	0,69	20,3	0,18	1,10	0,34	135	<L.D.	3,82	79,4	
InterBed F	24,8	23,3	8,70	0,11	0,02	11,8	264	1,60	8,4	19,8	7,28	2,84	0,05	<L.D.	5,00	18,6	5,82	255	0,18	14,34	1,22	25,2	0,31	1,23	0,53	147	<L.D.	9,00	83,5	
InterBed G	26,0	26,4	7,89	0,12	0,03	10,7	311	1,44	14,3	17,9	7,67	2,80	0,05	0,61	4,91	19,2	6,66	245	0,23	14,49	1,01	26,7	0,35	2,64	0,55	149	<L.D.	8,00	97,0	

Samples	La	Ce	Pr	Nd	Sm	Eu	Gd	Tb	Dy	Ho	Er	Tm	Yb	Lu	SiO ₂	Al ₂ O ₃	Fe ₂ O ₃	MnO	MgO	CaO	Na ₂	K ₂ O	TiO ₂	P ₂ O ₅	
	µg/g	µg/g	µg/g	µg/g	µg/g	µg/g	µg/g	µg/g	µg/g	µg/g	µg/g	µg/g	µg/g	µg/g	%	%	%	%	%	%	%	%	%	%	%
GG1	4,54	9,52	1,13	4,14	0,653	0,114	0,448	0,060	0,327	0,062	0,167	0,0258	0,182	0,029	51,06	10,34	17,16	0,016	3,59	0,53	0,05	6,98	0,36	<L.D.	
PR1	0,962	1,95	0,253	0,973	0,195	0,036	0,133	0,016	0,092	0,019	0,056	0,0088	0,064	0,010	47,47	5,44	27,47	<L.D.	2,73	0,20	0,03	8,09	0,49	0,17	
PR2	1,86	4,37	0,578	2,32	0,427	0,071	0,235	0,027	0,119	0,022	0,061	0,0095	0,068	0,010	47,66	5,50	27,41	<L.D.	2,73	0,20	0,03	8,12	0,053	0,17	
PR3	16,5	32,1	3,54	12,7	1,86	0,328	1,13	0,137	0,693	0,121	0,314	0,0459	0,336	0,052	50,89	10,10	16,76	0,021	3,52	0,58	0,06	6,78	0,73	0,13	
PR4	1,13	2,93	0,439	1,95	0,401	0,072	0,229	0,026	0,131	0,026	0,074	0,0111	0,084	0,012	47,62	5,48	27,17	<L.D.	2,74	0,19	0,03	8,14	0,053	0,16	
P1	18,3	43,5	5,74	23,0	4,39	0,772	2,76	0,350	1,91	0,378	1,05	0,157	0,985	0,148	49,39	7,34	22,97	0,017	2,42	0,31	0,08	7,06	0,24	0,27	
P2	21,7	54,1	6,95	27,6	4,99	0,829	2,77	0,299	1,40	0,235	0,596	0,0858	0,540	0,080	56,14	6,58	19,14	<L.D.	2,10	0,42	0,06	6,30	0,22	0,12	
T	1,08	2,92	0,276	1,06	0,207	0,041	0,168	0,023	0,134	0,025	0,065	0,0105	0,074	0,010	52,52	7,54	19,37	<L.D.	3,82	0,30	0,02	7,85	0,055	<L.D.	
SP	0,847	2,16	0,182	0,742	0,151	0,037	0,122	0,017	0,095	0,019	0,054	0,0070	0,057	0,008	51,61	7,46	20,15	<L.D.	3,84	0,31	<	8,03	0,051	<L.D.	
Cenom	0,922	2,32	0,209	0,794	0,156	0,032	0,137	0,017	0,096	0,019	0,047	0,0070	0,051	0,007	50,82	7,81	20,01	<L.D.	4,01	0,31	0,02	8,21	0,051	<L.D.	
Craie 1	12,113	23,23	3,004	12,262	2,474	0,554	2,216	0,316	1,834	0,356	0,922	0,1288	0,799	0,119	21,85	3,87	5,16	0,087	1,54	33,47	0,34	2,19	0,13	0,46	
Craie 2																									

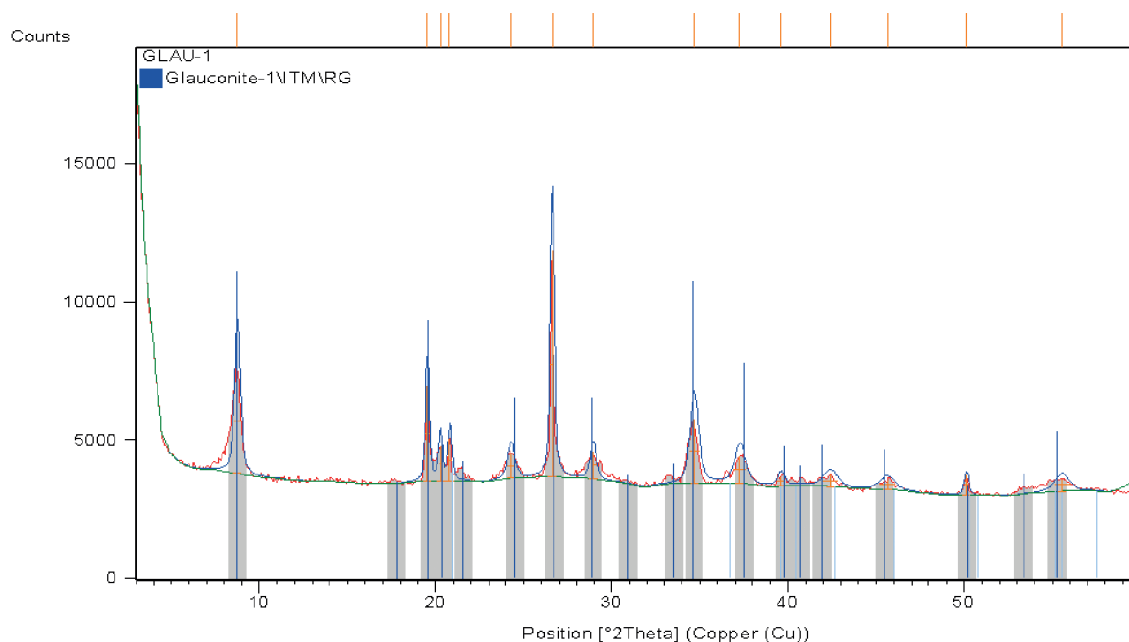
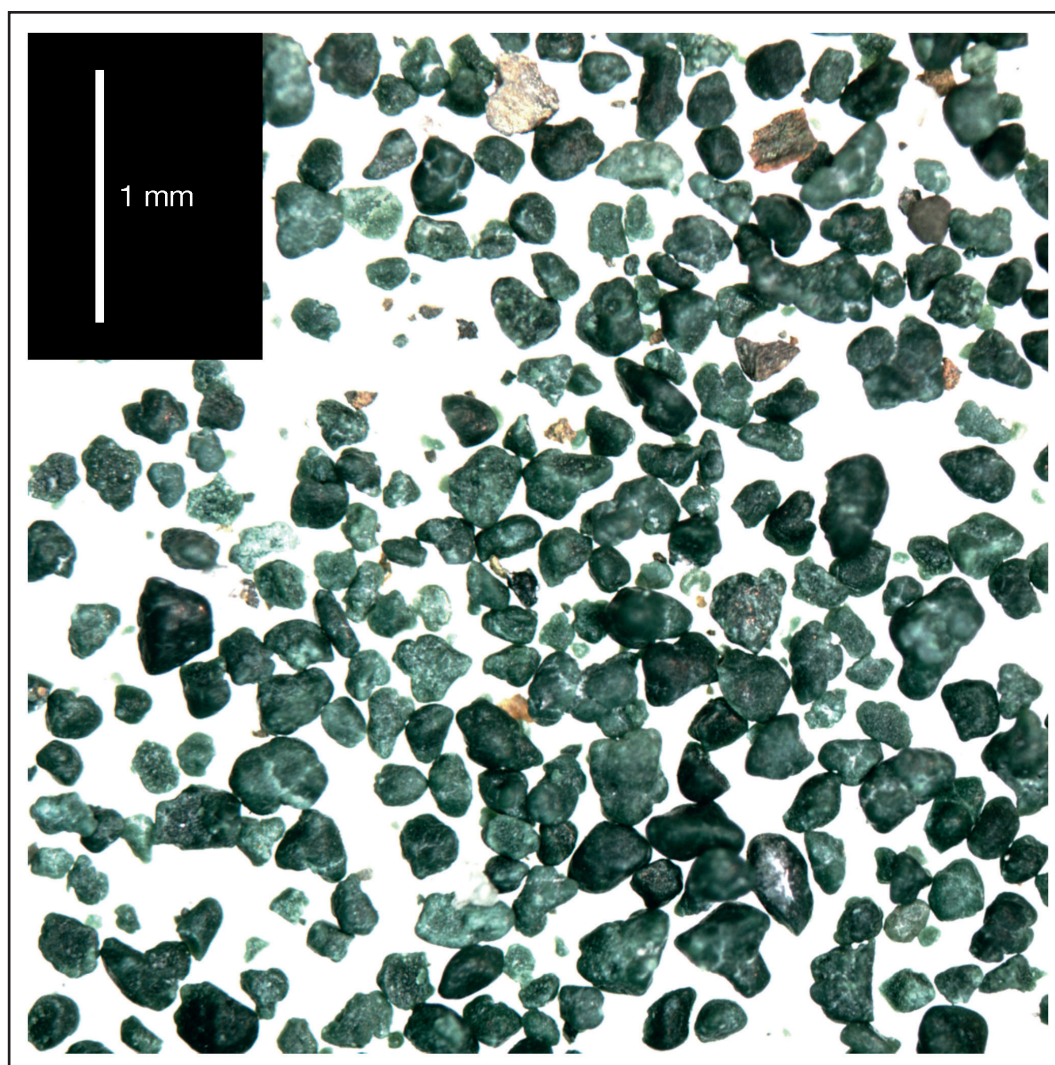


Fig. 2. (top) Typical diffractogram showing that all the green minerals studied are glauconite. Phase identification, based on peak positions (d-spacing) and relative intensities, has been performed on X-ray Diffraction patterns via Rietveld refinement (X'Pert high score Plus software - PDF4 database). The main peaks of the glauconite mineral appear at 2-Theta: 8.75 (100%), 34.60 (100%), and 19.58 (80%) at d-spacings of 10.100, 2.590, and 4.530 angströms, respectively.

Fig. 2. (en haut) Diffractogramme typique montrant que tous les minéraux verts étudiés sont de la glauconite. L'identification de phase, basée sur les positions des pics (espacement d) et les intensités relatives, a été réalisée sur les diagrammes de diffraction des rayons X via l'ajustement Rietveld (logiciel X'Pert high score Plus - base de données PDF4). Les principaux pics du minéral glauconite apparaissent à 2-Theta : 8,75 (100 %), 34,60 (100 %) et 19,58 (80 %) à des distances réticulaires d de 10,100, 2,590 et 4,530, respectivement (en Angströms).

Fig. 3. (bottom) Typical view of the glauconite grains observed in the various geological formation at stake in this work, using binocular microscope.

Fig 3. (en bas) Vue typique des grains de glauconite observés dans les différentes formations géologiques étudiées, au microscope binoculaire.



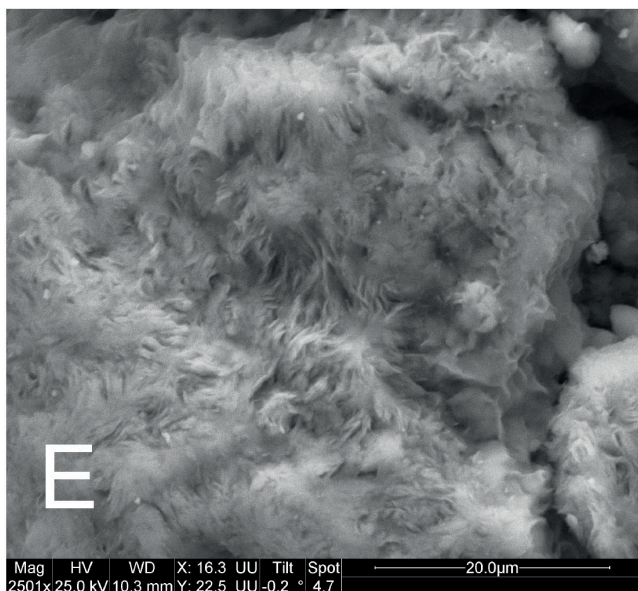
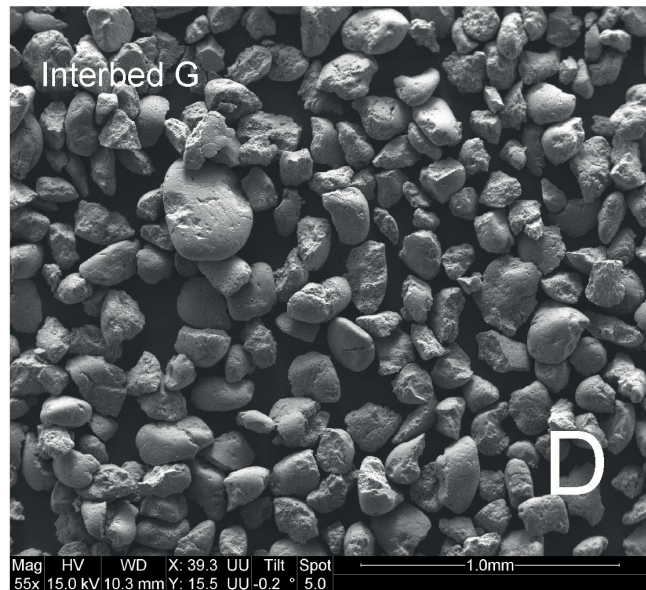
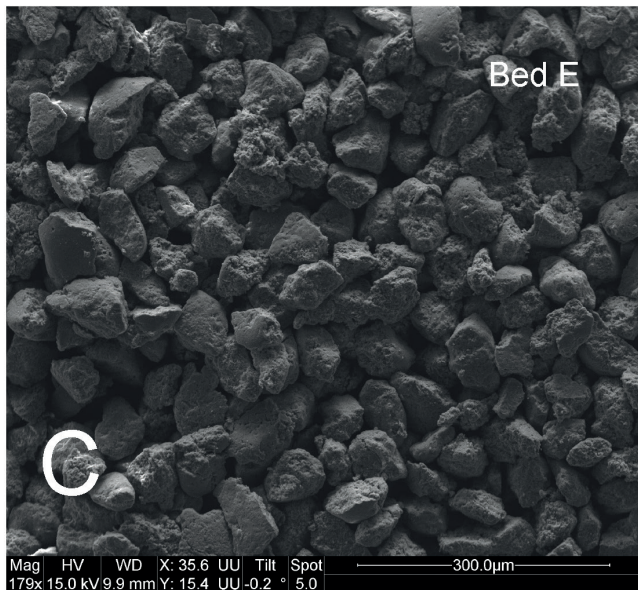
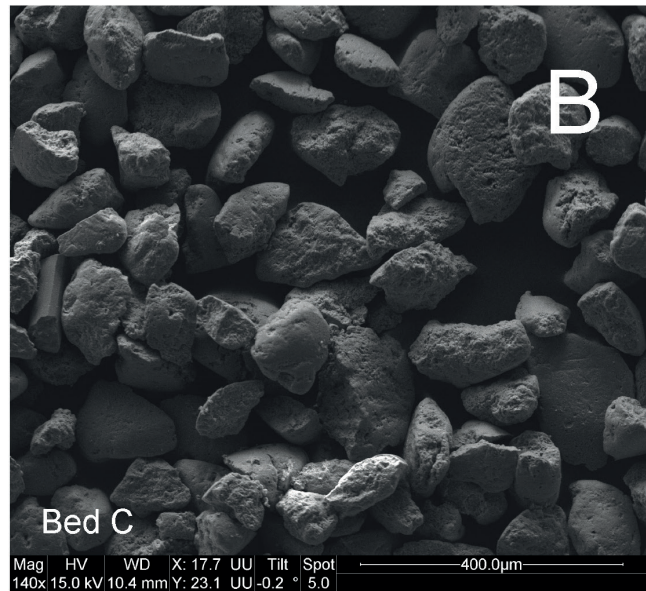
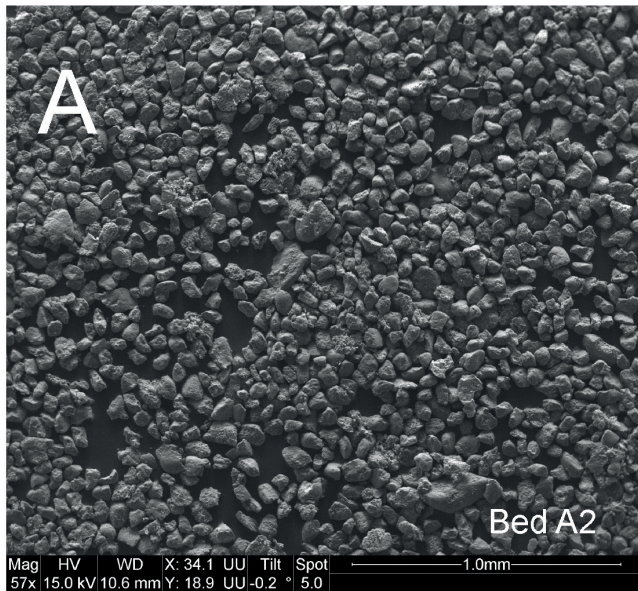


Fig. 4. SEM imaging of the morphologies of the grains. A, B & C: grains from carbonate beds; D: grains from a marly bed; E: rosette-like texture of the surface of some grains (samples PR, standing for patch reef).

Fig 4. Imagerie MEB des morphologies des grains. A, B & C : grains provenant de lits carbonatés ; D : grains d'un lit marneux ; E : texture en rosette de la surface de certains grains (échantillons PR, pour patch reef).

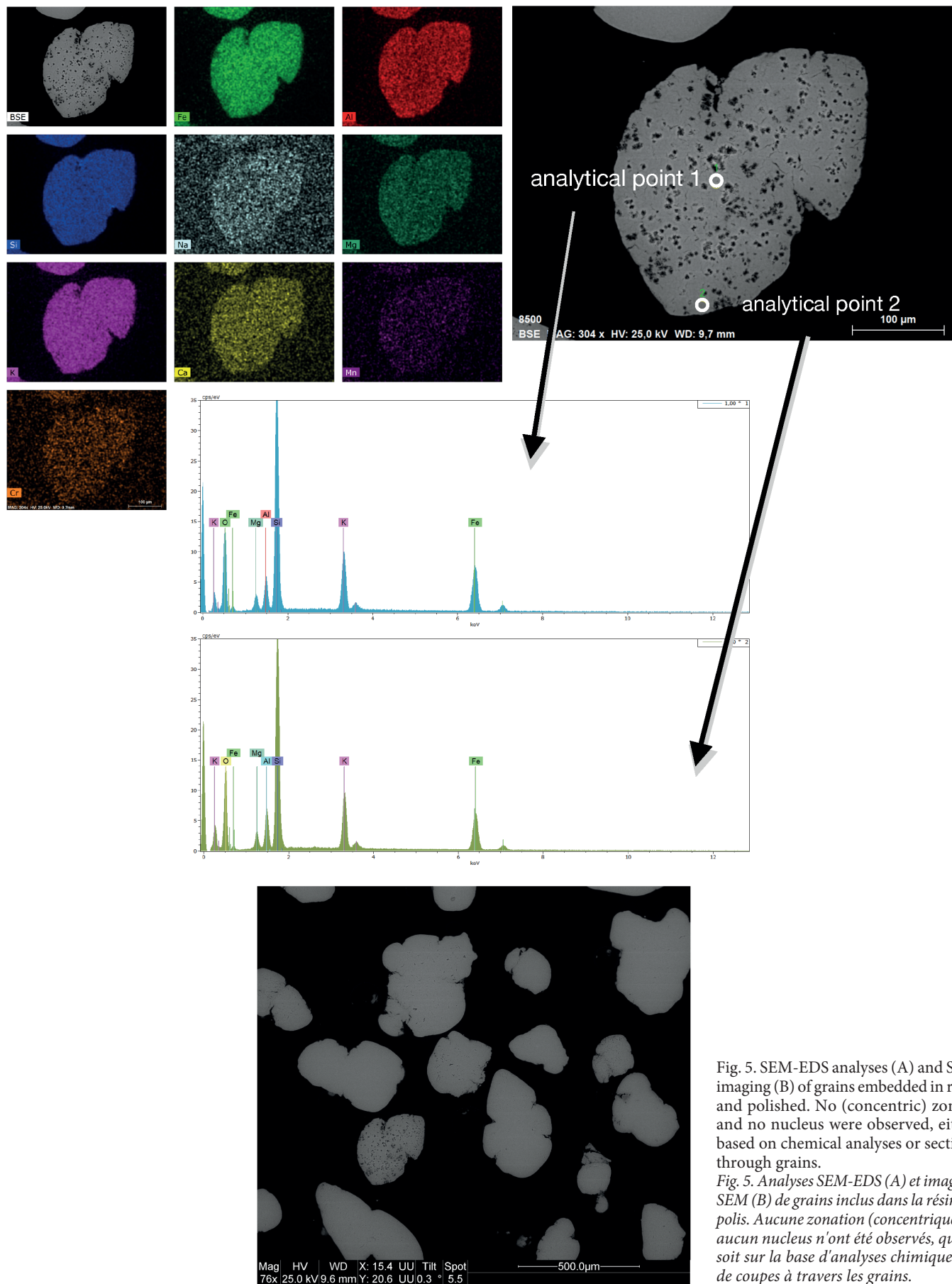


Fig. 5. SEM-EDS analyses (A) and SEM imaging (B) of grains embedded in resin and polished. No (concentric) zoning and no nucleus were observed, either based on chemical analyses or sections through grains.

Fig. 5. Analyses SEM-EDS (A) et imagerie SEM (B) de grains inclus dans la résine et polis. Aucune zonation (concentrique) ni aucun nucleus n'ont été observés, que ce soit sur la base d'analyses chimiques ou de coupes à travers les grains.

3. RESULTS

3.1. Precursors of the glauconite grains and degree of maturity

Observations of glauconite grains using light or electronic microscopes did not allow deciphering whether they could originate from foraminifer infilling or fecal pellets (Fig. 4 A-D). Colpaert et al. (2021), in their stratigraphic study based on foraminifers, did not mention the presence of glauconite-infilled foraminifers but their plate 2 shows the presence of some. In addition, regarding the chemical composition of glauconite, an important aspect is the nature and composition of the minerals acting as precursor phases of the authigenic growth. This consideration motivated thin sections to be cut through glauconite grains. Whatever the samples they came from, all the grains examined here through photonic microscopes and SEM imaging yielded homogeneous inner structure and composition (Fig. 5A, B): no possible precursor of glauconite, no zoning, but only homogeneous areas are observed (Fig. 5B). In addition to their composition in potassium and iron mentioned above, the grains exhibit a number of features indicating a high degree of maturity. Indeed, XRD always yields glauconite diffractograms with well-defined peaks, to be related to a high crystallinity. Through SEM imaging, some grains showed rosette textures on the surface (Fig. 4E). Rosette-like structures are a marker of maturity according to Lopez-Quiros et al. (2019), Banerjee et al. (2012b) or Roy Choudhury et al. (2021b, 2023). A dark-green color together with the presence of cracks is commonly associated to a high degree of maturity (Giresse et al., 2021; Roy Choudhury et al., 2021b, 2023).

3.2. Distribution of the samples in two sets

In what follows, the analytical results are illustrated and interpreted in two separate sample sets. The set 1 groups glauconites of various ages and depositional environments (#1, 2, 4 and 6 of Fig. 1 and Table 1). They have been examined by Tribovillard et al. (2021, 2023a). The geological formations where these samples come from are summarized in Table 1. They span a facies range from oyster reefs to chalk via silty marls and green sands, and an age range from the Kimmeridgian/Tithonian to the Cenomanian. The deepest depositional settings correspond to the Cenomanian chalk, the other ones range between shallow shoreface and (lower?) offshore, as detailed in Tribovillard et al. (2021, 2023a). The set 2 groups the samples of limestone beds and marly beds from the Assises de Croï Fm (Tribovillard et al., 2023b; #3 of Fig. 1). The Assises de Croï Fm is dated as upper Tithonian (Albani, Glaucolithus and Okusensis ammonite zones; Townson & Wimbledon, 1979; Tribovillard et al., 2023b and references therein). With a thickness of ca. 10 m, the Assises de Croï Fm yields nodular, glauconitic limestones alternating with silty, glauconitic marls (Fig. 6 next page). This second

sample set therefore contains glauconite grain populations of the same age and deposited under the same energy and depth conditions, they differ only in their host-rock facies (limestone versus marl), expressing contrasted diagenetic processes. Separating the samples into two sets allows the interpretations to be drawn at contrasting scales: the set 1 will permit interpretations about glauconite populations spanning various depositional settings and ages, whereas the set 2 will allow the focus to be set upon small variations at closer scale.

3.2.1. Sample set 1.

The K_2O contents of the glauconite samples are relatively high, distributed between 2% and 9%, most often above 6% (Fig. 7). Only the chalk samples Craie1-4 rank below 6%. This figure illustrates that most of the samples may be considered to be highly mature, according to usual nomenclature (K_2O above 8%). The K_2O contents correlate remarkably well with Rb contents ($R^2 = 0.97$; Fig. 8A). In other words, the excellent correlation between K_2O and Rb is not altered by the contrasting ages and depositional settings of the samples analyzed (see below). As regards REE, no striking point can be put forward. If we consider all the REEs, we see that the parameter ΣREE brings out from the set of samples the glauconites contained in four chalk samples (Craie 1-4) as well as the two condensed levels rich in phosphate shells (P1 & P2) and one of the four patch reefs studied (PR3; Fig. 8B shaded area). All other samples show comparatively much lower ΣREE . The patterns of REE established from glauconite grains are grouped in Figure 9A. No marked tendency stands out. Anomalies in Ce and Eu are not very marked; those in Eu are usually weakly positive, those in Ce are weakly positive or negative. The (La/Lu)_N ratio shows a fairly wide range of values, the values of the (La/Sm)_N ratio are more narrowed and a wider range of values is observed for the (Gd/Yb)_N ratio. Noteworthy, the contents (normalized or not) of Nd and Sm are closely correlated, whatever the origin of the samples (age, depositional setting). The correlation linking Sm and Nd is classical but, here, it is unaffected by the depositional or diagenetic conditions (Fig. 8C). As regards redox-sensitive trace elements, the glauconite samples of the sample set 1 show relatively high contents in vanadium (V) and chromium (Cr), these elements yielding some positive correlation (Fig. 8D). In the same way, although germanium (Ge) concentrations do not exceed 10 ppm, they generally show a fair correlation with V concentrations (Fig. 8E).

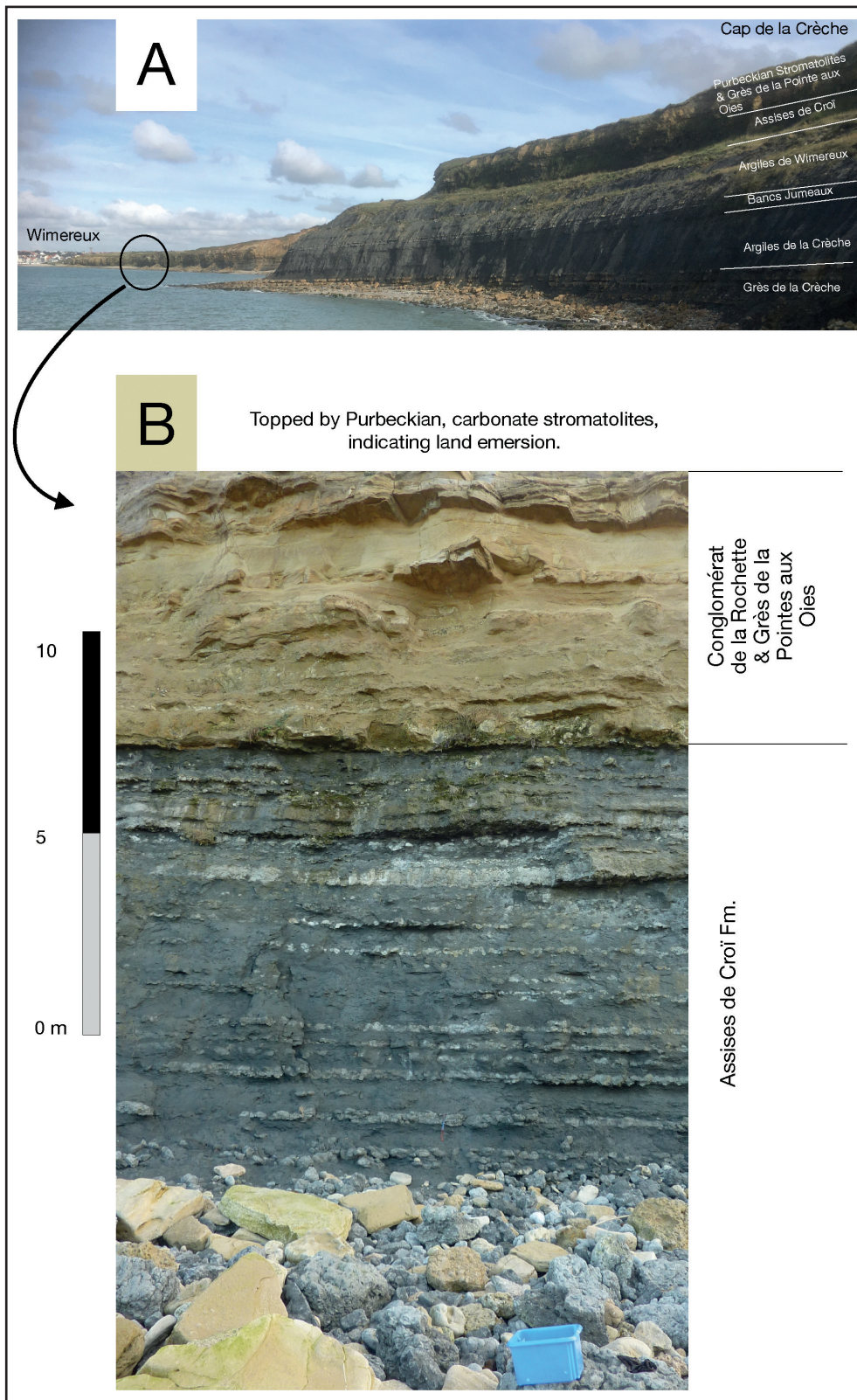
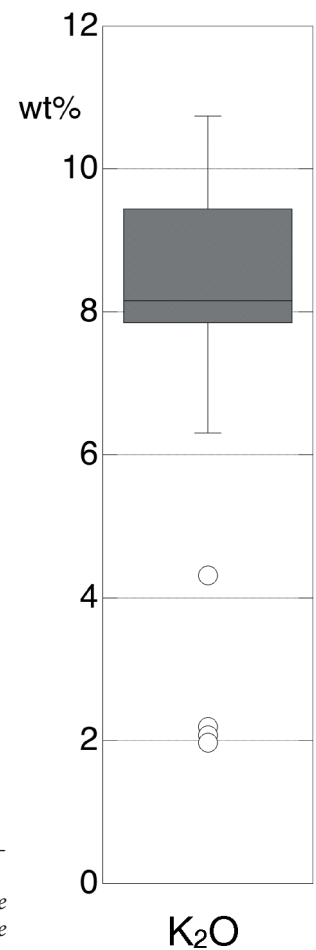


Fig. 6. View of the Assises de Croi Fm pictured between the city of Wimereux and the small cape called Rochers du Fort de Croi (A), located at mid-distance between Wimereux and the Cap de la Crèche (map in Fig. 1). B: the facies of the limestone-marl alternation. The formation was pictured south of Wimereux because there, the outcrop forming a clear-cut cliff, but it was sampled north of Wimereux (Pointe de la Rochette) where the outcrop is more accessible. Photo used in A was already used in a composite picture of Tribovillard et al. (2023a, their Figure 2).

Fig. 6. Vue des Assises de Croi Fm photographiée entre la ville de Wimereux et le petit cap appelé Rochers du Fort de Croi (A), situé à mi-distance entre Wimereux et le Cap de la Crèche (carte fig. 1). B : le faciès de l'alternance calcaire-marne. La formation a été photographiée au sud de Wimereux car là, l'affleurement forme une falaise nettement découpée, mais elle a été échantillonnée au nord de Wimereux (Pointe de la Rochette) où l'affleurement est plus accessible. La photo utilisée en A était déjà utilisée dans une image composite de Tribovillard et al. (2023a, leur figure 2).

Fig. 7. Box diagram of the K₂O concentrations measured on 45 samples of glauconite (this work plus non-published analyses), showing that most samples rank beyond 8 wt%.

Fig. 7. Diagramme encadré (ou diagramme en boîtes) des concentrations de K₂O mesurées sur 45 échantillons de glauconite (cette étude + analyses non publiées), montrant que la plupart des échantillons se situent au-delà de 8 % en proportions pondérales.



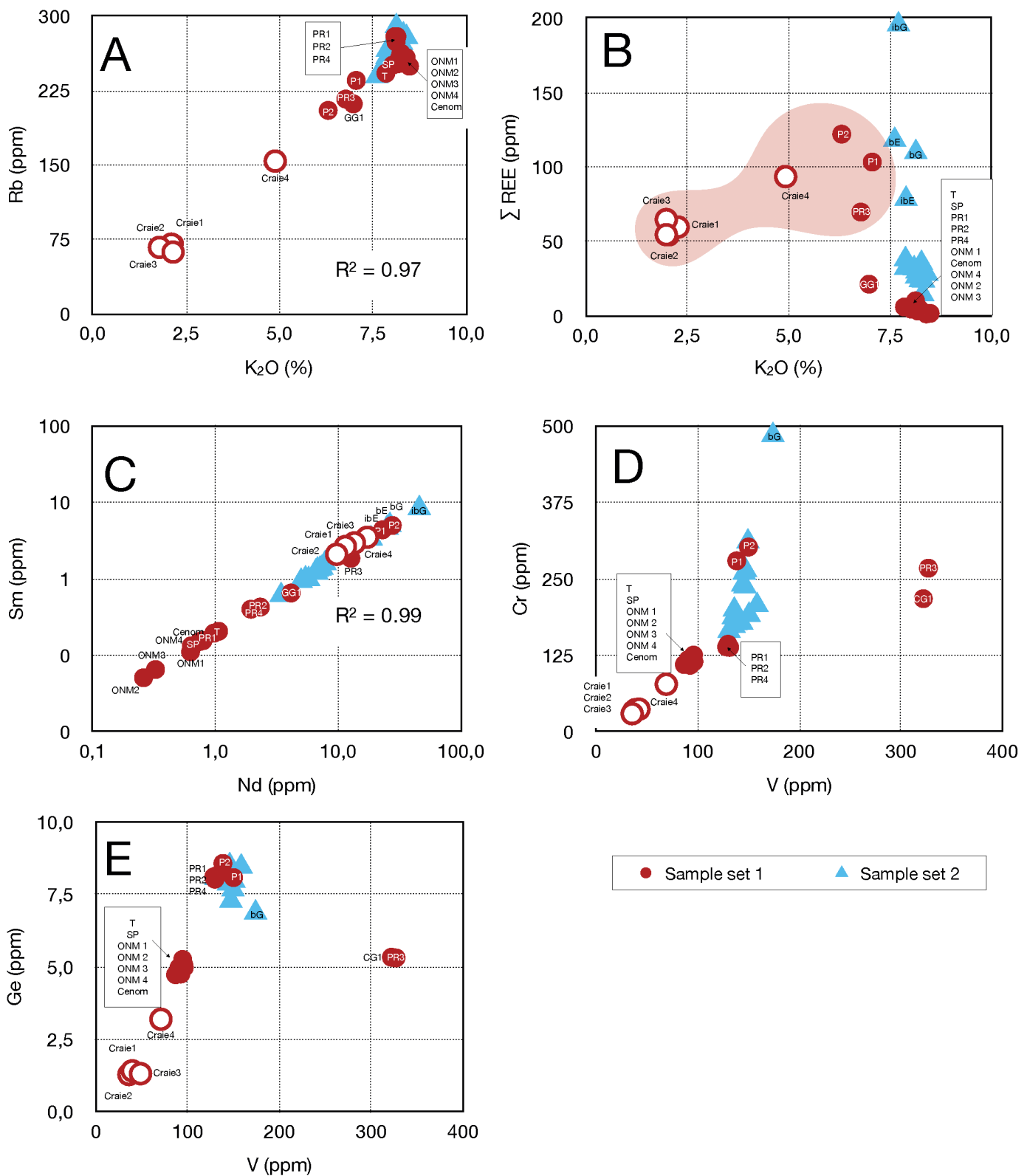


Fig. 8. Various cross diagrams illustrating the respective samples of the two sets examined here. A: K_2O versus Rb; B: K_2O vs. ΣREE ; C: Nd versus Sm; D: V vs. Cr; E: V versus Ge. The samples of set 1 are all labelled; only the outliers of sample set 2 are labelled, for the sake of readability of the picture. Sample names are indicated in Fig. 1.

Fig. 8. Divers diagrammes croisés illustrant les échantillons respectifs des deux ensembles examinés ici. A : K_2O versus Rb; B : K_2O versus ΣREE ; C : Nd versus Sm; D : V versus Cr; E : V versus Ge. Les échantillons de l'ensemble 1 sont tous étiquetés; seules les valeurs aberrantes de l'ensemble d'échantillons 2 sont étiquetées, par souci de lisibilité de l'image. Les noms des échantillons sont indiqués sur la figure 1.

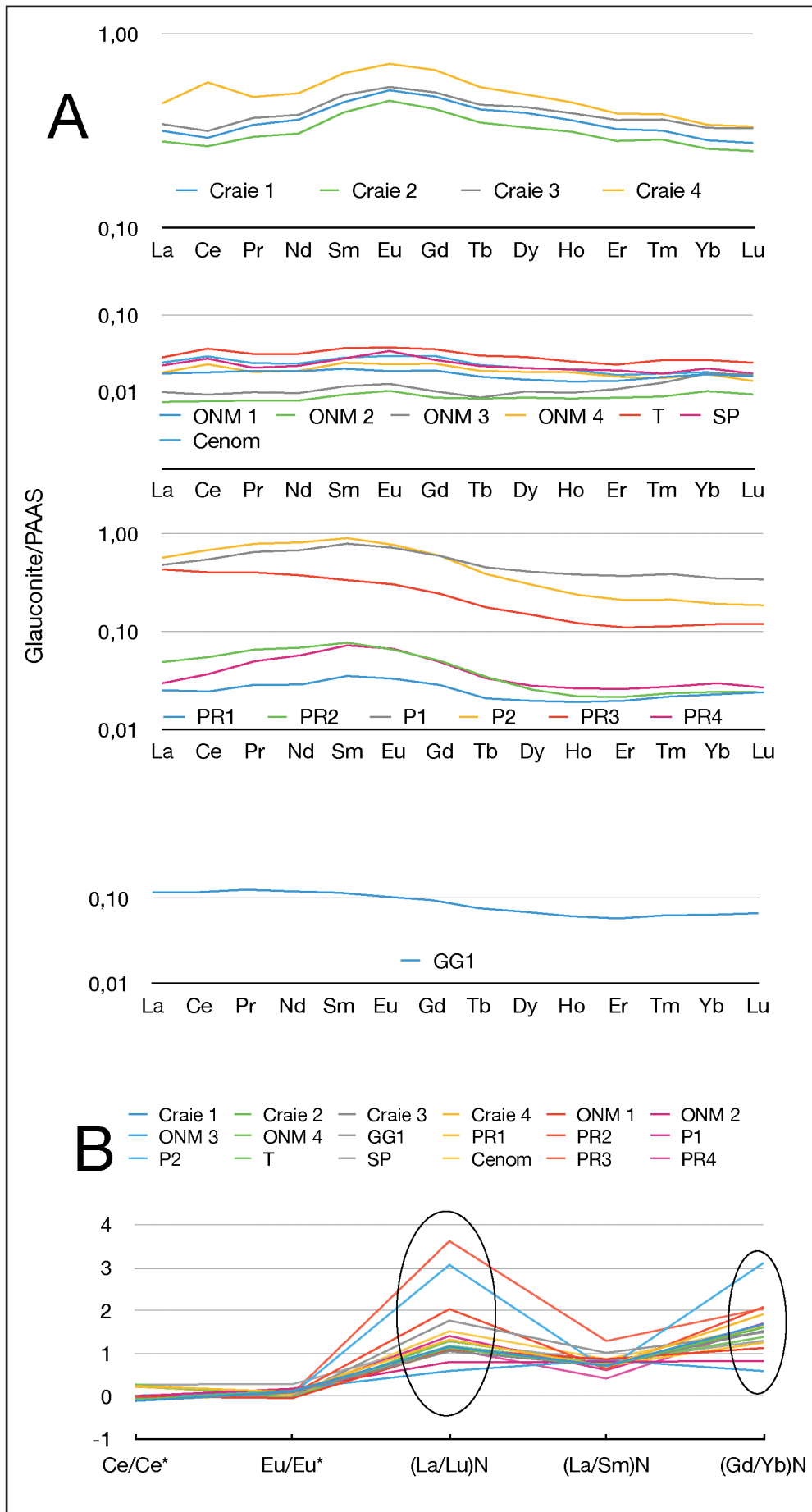


Fig. 9. Rare earth element (REE) patterns (A) and parameters (B) of sample set 1. Sample locations are indicated in Fig. 1. B: Distribution of values of REE parameters commonly used to describe patterns (A). These are the cerium and europium anomalies, as well as the ratios characterizing light, medium and heavy REE, respectively. The ellipses show that the most variable parameters are (La/Lu)N and (Gd/Yb)N; for easier reading, see the values table 2.

Fig. 9. Patterns de Terres Rares (REE) (A) et paramètres (B) de l'ensemble d'échantillons 1. Les localisations des échantillons sont indiquées sur la figure 1. B : Distribution des valeurs des paramètres de Terres Rares communément utilisés pour décrire les patterns (A). Il s'agit des anomalies en cérium et en europium, ainsi que des rapports caractérisant les Terres Rares légère, medium et lourdes, respectivement. Les ellipses montrent que les paramètres les plus variables sont (La/Lu)N et (Gd/Yb)N; pour une lecture plus aisée, voir le tableau de valeurs 2.

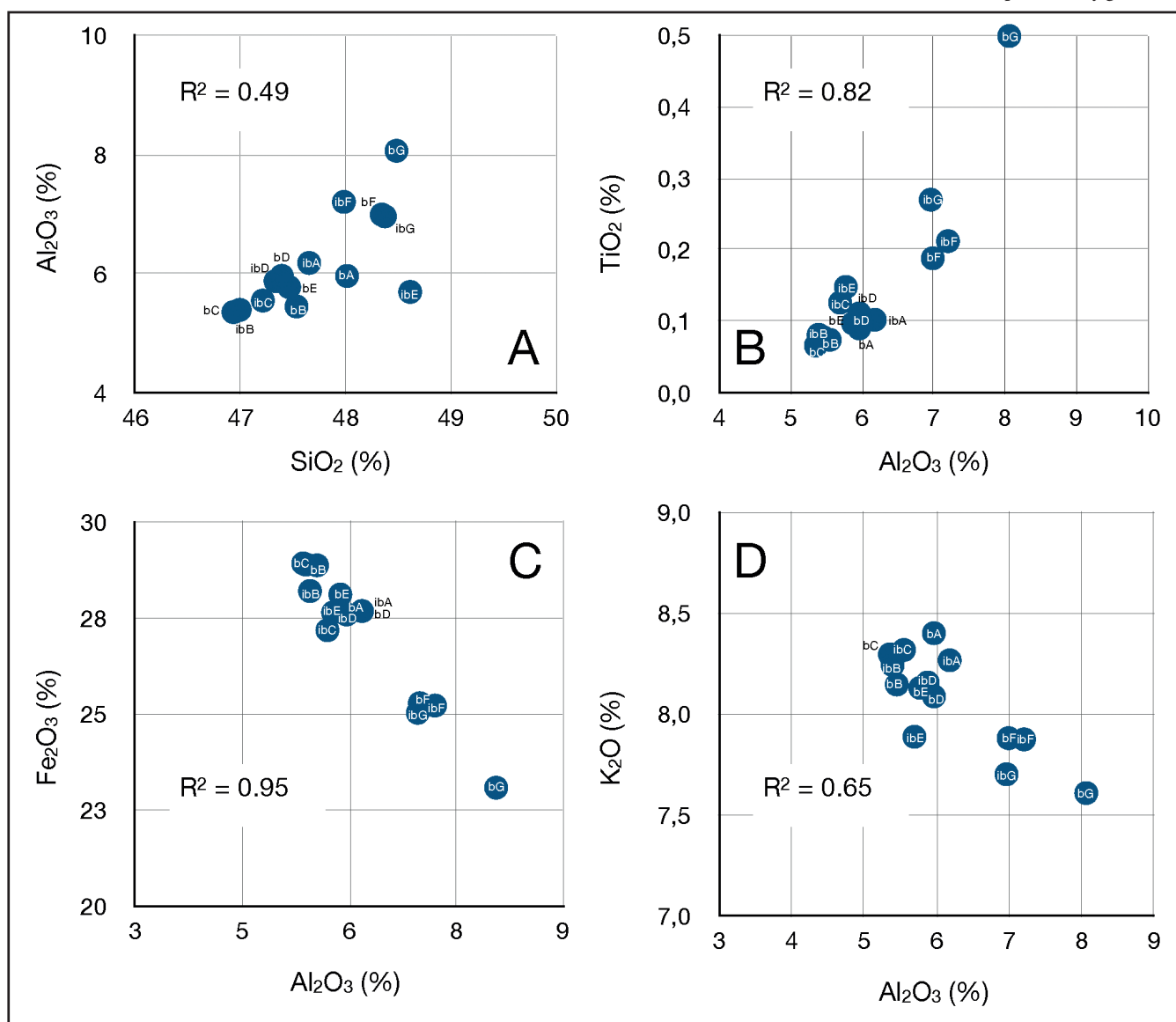
3.2.2. Sample set 2.

As for the sample set 1, the glauconites of the sample set 2 show relatively high concentrations in V and Cr, with the respective concentrations of the two elements being correlated. With respect to Ge, the glauconites of the set 2 plot in the V vs. Ge diagram of Figure 8E consistently with the ones of the set 1. The most striking correlations are observed between Nd and Sm from one part, and K_2O and Rb from the other part (Fig. 8A, C). In addition, a negative correlation is observed between Al, from one side, and K_2O or Fe_2O_3 from the other side (Fig. 10), while a positive correlation is seen between Al vs. SiO_2 and TiO_2 (Fig. 10A, B). It indicates that iron and potassium, two key elements with regard to glauconite growth, are not simply inherited from the precursor aluminosilicate nucleus the authigenic growth started on. Therefore, part of the content in both metals must have been captured from seawater during authigenesis. As for the glauconite of Set 1, no obvious relation is observed between K_2O and ΣREE (Fig. 8B).

Figure 11A, B allows to compare the respective REE patterns of the carbonate and marly beds of the Assises de Croi Fm. The most visible features do not concern the carbonate vs. marly beds comparison, but instead three samples (E, F, and G). differ from their companion samples, either for carbonate vs. marly beds (Fig. 11A, B). In other words, differences are more stratigraphic than lithologic. The redox-sensitive trace metals considered here do not yield any observable trend, with neither contrast between carbonate vs. marly beds, nor stratigraphic distributions.

Fig. 10. Various cross diagrams illustrating the samples of the set 2 (Assises de Croi). A : SiO_2 versus Al_2O_3 ; B : Al_2O_3 vs. TiO_2 ; C : Al_2O_3 vs. Fe_2O_3 ; D : Al_2O_3 vs. K_2O . Sample labels: b stands for carbonate bed, ib stands for marly interbed. Sample locations are indicated in Fig. 1

Fig. 10. Différents diagrammes croisés illustrant les échantillons de l'ensemble 2 (Assises de Croi). A : SiO_2 contre Al_2O_3 ; B : Al_2O_3 contre TiO_2 ; C : Al_2O_3 contre Fe_2O_3 ; D : Al_2O_3 contre K_2O . Etiquettes des échantillons : b signifie lit (i.e., bancs carbonatés), ib signifie interlit (i.e., interlits marneux). La localisation des échantillons est indiquée sur la figure 1.



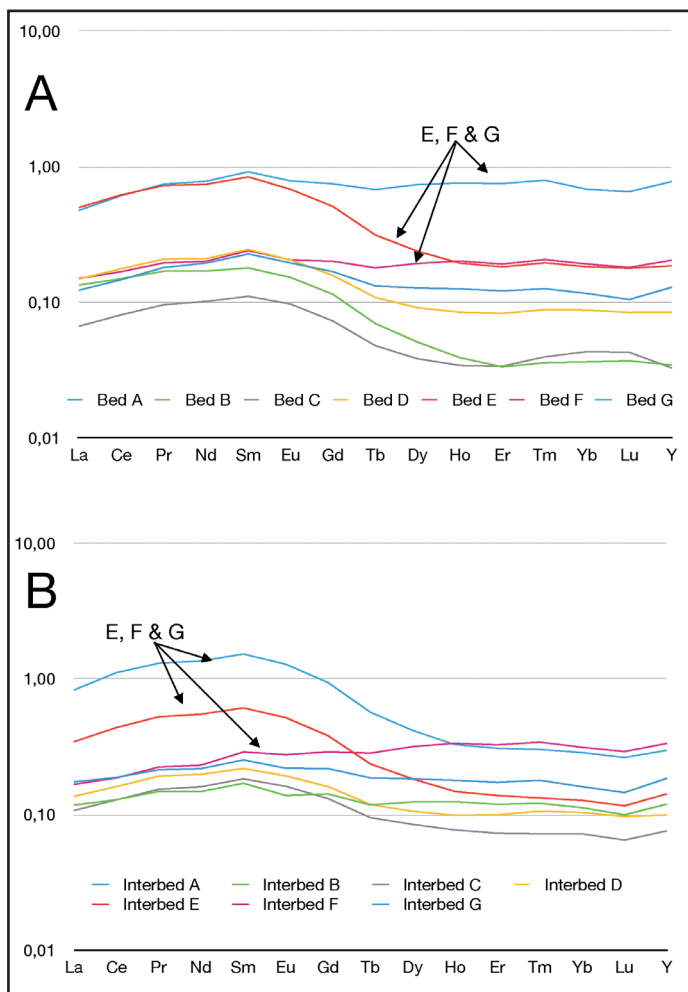


Fig. 11. REE patterns of sample set 2. A: carbonate beds; B: marlstone beds (Assise de Croï Fm). Sample locations are indicated in Fig. 1.
 Fig. 11. Patterns de Terres Rares (REE) de l'ensemble d'échantillons 2. A : bancs carbonatés; B : lits de marnes ou interbancs marneux (Assise de Croï Fm). Les localisations des échantillons sont indiquées sur la figure 1.

4. INTERPRETATIONS

4.1. REE distribution and signs of maturity

Previous works (Fleet et al., 1980 and references therein; Stille & Clauer, 1994; Kechiched et al., 2018) have shown that authigenic minerals exhibit relatively complex partitioning with respect to seawater, regarding REEs. Using selective chemical extractions, Zhang and Shield (2023) confirmed the mobility of REE during early diagenesis in marine sediments. It is established that seawater has a deficit in Ce for redox reasons and the minerals formed in the ocean environment record this deficit (e.g., Piper, 1974; Murray et al., 1990; Sholkovitz & Schneider, 1991; Wilde et al., 1996; Tostevin et al., 2016). However, Fleet et al. (1980) report that this deficit does not appear in authigenic minerals formed in shallow marine environments. Glauconites from shallow seas sometimes even show weakly positive anomalies, which are attributed to

the fact that glauconite preferentially incorporates Ce from seawater (sort of “cerium pump”). Similarly, seawater is relatively enriched in heavy REEs, due to the propensity of these REEs to form soluble complexes; however, this enrichment is not observed in authigenic minerals from shallow marine environments (Fleet et al., 1980; Deng et al., 2017).

The potassium content (K_2O) is a classic marker of glauconite maturity used by many authors following the pioneering work of Odin & Matter (1981). A K_2O content above 8 wt% together with a Fe_2O_3 concentration of 24%–28% is the signature of the highly evolved glauconite, the formation of which lasting over a few hundred of kyrs, or even about one million yrs. Here, the K_2O and Fe_2O_3 concentrations of the samples studied correspond predominantly to highly mature glauconite. It may be stressed that some glauconite grains of the patch reefs (samples PR) show rosette-like structures (Fig. 4E). Such structures correspond to evolved but not highly evolved stages of glauconite development, according to Banerjee et al. (2019), Oze et al. (2019), Roy Choudhury et al. (2021b) and Singh et al. (2023). The rosette-showing grains have, however, high concentrations in iron and potassium. This discrepancy could be accounted for by the fact that these samples come from oyster patch reefs that worked as a sort of glauconite factory (Tribovillard et al., 2023a). The patch reefs developed at, or close to, cold-seep vents (Hatem et al., 2016). Cold seep fluids may be sources of dissolved iron and potassium (Suess, 2014; Olu et al., 1996; Wang et al., 2017, Zhang et al., 2022). Therefore, as the glauconites of the samples PR grew close to sources of Fe and K, they might have been enriched in both metals even if the rosette structures suggest a lesser degree of maturity. Last, Banerjee et al. (2019) and Oze et al. (2019) noted that such structures may be linked to infilling (e.g., of foram chambers); however the morphologies of the grains observed in the present study did not allow such a conclusion (which does not rule out the infilling hypothesis).

Tribovillard et al. (2023b) identified precocious glauconite, that formed prior to the hosting, early-diagenetic limestone beds, although showing the geochemical characteristics of evolved glauconite. In other words, glauconite could form during earliest diagenesis in a shallow depositional setting where sedimentation rates were substantial, and yet it bears all the physical and geochemical characteristics of a glauconite supposedly grown during protracted durations. This paradox evidences that the K_2O content cannot be considered any longer to be automatically a reliable tracer of the duration of formation for glauconite (see also Chafetz & Reid, 2000). Therefore, it may be of interest to know whether REEs can be an alternative marker for this process. To examine the trace-element content as a marker of diagenetic conditions, the question about the nature of the precursor phase must be addressed: the K_2O content of a glauconite may be impacted if the precursor is a K-feldspar. In such a case, using the K_2O

concentration as a maturity proxy may be pointless. From the X-ray diffractograms yielding pristine glauconite, the mineralogical nature of the precursors could not be inferred. Examining the inner structure and composition using SEM did not help either in the determination of the precursor phases. Finally, in the present case, all the glauconite grain samples studied except for the 4 bulk-rock chalk samples Craie1 to Craie4 show a high K_2O content (Fig. 7). However, it is highly unlikely that all the remaining samples all had a K-rich precursor. Therefore, we are unable to discuss the role possibly played by the precursor phases in the composition of the studied glauconite samples but our results suggest that their K richness cannot be ascribed to a single type of precursor; consequently, it will be considered that the K_2O content can be used as a marker of the degree of evolution of glauconite. Accordingly, the possible influence of the precursors upon the trace element composition cannot be meaningfully discussed.

Regarding the sample set 1, the ΣREE factor is not correlated with the K_2O concentration, but it is observed that the samples which are the richest in phosphate nodules are also those showing the highest ΣREE (7 samples: 4 chalk samples Craie1 to 4, the P1 & P2 levels of the Bancs Jumeaux Formation and one patch reef PR3; Fig. 8B, shaded area). Noteworthy, the concentrations in P_2O_5 and ΣREE are not correlated, and yet the usual presence of REE in phosphorites is well documented in the literature (Kechiched et al., 2018 and references therein). Regarding the seven samples mentioned above, the chalk samples come from the Cenomanian levels which underwent a very pronounced rise in sea level accompanied by a strong decrease in the rate of sedimentation (Amorosi & Centineo, 2000; Amédro & Robaszynski, 1999). Similarly, levels P1 & P2 correspond to prolonged gaps of sedimentation (Geysant et al., 1993; Deconinck et al., 1996; Deconinck and Baudin, 2008) of a duration estimated to be in the order of one or two ammonite zones (Hudlestoni and Pectinatus). Thus, these six samples correspond to the most condensed episodes of sedimentation among all the cases studied in this work; it is therefore proposed that the sedimentation slowdowns are associated with an increase in the REE content of authigenic glauconite, in relation to the prolonged exchange times between the seawater and the glauconite grains being growing authigenically. Beyond the ΣREE parameters, are specific distributions of REEs observable in the patterns? Three of the four chalk samples show a slight negative anomaly in Ce (samples Craie1–3, Fig. 9), which could suggest that the glauconites had more time to incorporate Ce from the seawater. Nevertheless, the same figure illustrates that this anomaly is not observed for the fourth chalk sample and no heavy-REE enrichment is recorded in any of the four samples. The same goes for P1 & P2, showing neither Ce anomaly, nor enrichment in heavy REE. Thus, the glauconites that formed under conditions

of low sedimentation rate did not play any role of “sink” for Ce and heavy REE. The other samples show hardly any interpretable trends. A slight enrichment in intermediate (medium) REE is observed for a certain number of samples (convex-up shape from La to Tb, Fig. 9). Such enrichment has already been observed by Fleet et al. (1980) and seems to be common for glauconite, without the authors offering any interpretation.

In short, on the basis of the first set of samples examined here, illustrating different depositional conditions, varying sedimentation rates and contrasted ages, it appears that the REE patterns of the glauconites do not allow for the identification of interpretable trends. At best, it is observed that the total REE content (ΣREE) was higher when sedimentation rates were lower. This absence of interpretable trends in the distribution of REEs may be attributable to sampling heterogeneity. To compare samples of ages that are too far apart, or deposited in contexts differing from each other by too many parameters might not be relevant. To test this hypothesis, a second set of samples was taken into consideration. It is restricted to samples from the same formation (the Assises de Croi Fm) and therefore of approximately the same age and deposited under similar conditions (upper offshore). In addition, these similar conditions suggest that the regional-scale seawater composition may have been stable during the entire deposition of the alternating facies. However, regarding most specifically the sample set 2, the results illustrated with Figs. 8 and 11 do not allow any interpretation to be drawn, as far as REE and ΣREE are considered. No tendency could be observed, considering the samples of the carbonate or marly beds, or mixing all the samples. REE examination does not yield any significant support.

4.2. K_2O vs. Rb, Sm vs. Nd

For all the samples of glauconite studied (sample sets 1 & 2), the chemical analyses make it possible to draw remarkable correlations between the contents of K_2O and those of rubidium (Rb) on the one hand, and between the contents of samarium (Sm) and those of neodymium (Nd), on the other hand (Fig. 8). Regarding most specifically the sample set 2, the concentrations in K_2O and Rb on the one hand, and Nd and Sm on the other hand, plot at a consistent location in a K_2O vs. Rb diagram or Nd vs. Sm diagram, respectively: expectedly, the samples of Set 2 are grouped in these diagrams, in agreement with their similar origin (close in time and space), compared to the samples of Set 1. Substitution of K by Rb is common in glauconite as in many other minerals (e.g., Wiewiora & Lacka, 1985, and, more recently, Rafiei et al., 2023). The Sm-Nd couple is mainly studied for the purposes of isotopic dating but the concentrations of these two elements have hardly been examined as far as we know (Rafiei et al., 2023). The striking feature of our results is that in the two diagrams K vs. Rb and Sm vs. Nd (Fig. 8), the

points align almost perfectly while the glauconites analyzed are quite heterogeneous with regard to both their age (Tithonian, Aptian-Albian, Cenomanian) and their environments of formation. Thus, despite these disparities, K and Rb on the one hand, and Sm and Nd on the other hand, were incorporated in the same proportions in the authigenically growing glauconite. This suggests that differences in the chemical composition of the seawater as well as that of the sediments did not impact the crystal chemistry of glauconite: diadochic substitutions thus seem to have obeyed very strict rules. This is interesting in as much as it is thus suggested that glauconite is not a mineral with loose specifications depending on the ambiance it grows in during early diagenesis: whatever the duration of authigenic growth and the variations in (interstitial) seawater composition that may have occurred between the Tithonian and the Cenomanian in the Boulonnais, glauconite yields constant proportions between K and Rb, and Sm and Nd. Several explanations may be put forward. The equilibrium between K_2O and Rb, and between Sm and Nd, may be interpreted as the indicator of high maturity, from a crystallochemical point of view, which demands time. To illustrate this statement, the strontium abundance of carbonates may be considered. Fast forming aragonite or calcite incorporate Sr in important and variable proportions, whereas slow-forming or recrystallized calcite has Sr low contents that fall into rather narrow concentration ranges (Morse & Mackenzie, 1990). In other respects, the outstanding correlations shows that neither ‘fractionation’ nor sort of ‘Rayleigh distillation’ occurred between the two pairs of elements. It is inferred that the glauconite growth took place in close contact with an ‘infinite reservoir’ of dissolved elements (Rb, K, Nd, Sm), that is, the open seawater reservoir. With the proximal depositional settings described here, where sedimentation rates must have been relatively high, unhindered contacts with marine water masses imply that authigenic growth must have been (relatively) rapid. However, ‘earliest diagenesis’ does not necessarily implies ‘shortest duration’: the glauconite at stake here may well have formed during the earliest stages of diagenesis but the process may have lasted quite long (J.-F. Deconinck mentions evidences for some depositional gaps within the Assises de Croï Formation; personal communication 2024). The words early or late diagenesis express here a chronological succession with no precise quantification of duration. Although no quantitative data regarding the duration of glauconite growth are available here, it may be stated that, from a qualitative point of view, the depositional settings discussed here were shallow (at most lower offshore) and, thus, the sedimentation rate was probably not null. Consequently, even if long periods of growth might be envisioned in such shelfal settings, these durations are not likely to be extreme. A way to reconcile the need for a long time of growth accompanying episodes of condensed sedimentation (van Houten & Purucker, 1985;

Föllmi, 2016) and proximal settings with possible relatively high sedimentation rates would involve the role played by winnowing processes (Giresse & Wiewiora, 2001; Föllmi, 2016). Proximal settings may witness episodes of condensation prone to formation of glauconite, and episodes of deposition, with glauconite being concentrated through winnowing.

4.3. Redox proxies of the two sample sets

The glauconites of the two sample sets show rather high concentrations in both V and Cr (both being correlated) and a correlation between V and Ge. Vanadium is a long-known redox-sensitive element that has been intensively studied (Breit & Wanty, 1991; Wanty & Goldhaber, 1992; Tribovillard et al., 2006; Meunier, 1994; Huang et al., 2015; Gustafsson, 2019; Haase et al., 2024). Vanadium is also known to be incorporated into phyllosilicates during diagenesis in a reduced stage (Huang et al., 2015; Gustafsson, 2019). Therefore, as formation of glauconite has been proved to take place during earliest diagenesis in the Assises de Croï Fm, V concentrations must be a reliable marker of the redox conditions developing at the sediment-water interface (or close to it), during the initial stages of diagenesis/authigenesis.

Germanium (Ge) has been proven to be redox sensitive in sedimentary environments (Tribovillard et al., 2011, 2021), during its substitution to Si in silicates (e.g., Rouxel et al., 2006; Tribovillard, 2013). Therefore, the correlation between V and Ge in glauconites is quite logical in the present case. Chromium is also reputed to be redox sensitive (to some extent) and to be brought to the sediments together with organic matter (Tuttle et al., 2009; Semeniuk et al., 2016). Bruggmann et al. (2023) recently insisted on the importance of the role played by organic matter in the enrichment of the sediment in Cr. In the present case, organic matter is lowly abundant in the deposits of the Assises de Croï Fm (TOC < 0.5%; Tribovillard et al., 2023b). In addition, Rock Eval pyrolysis showed that the organic matter is of Type III, that is, most probably issued from terrestrial organic products or degraded marine organic matter. Thus, the richness in V, the paucity of organic matter, the absence of well-preserved marine organic matter strongly suggest that bottom conditions were reducing and marine productivity was modest. With such reducing redox conditions, high productivity would have expectedly induced significantly higher TOC values and the presence of Type-II organic matter, which is not the case. Consequently, under depositional conditions characterized by reducing conditions and low organic supply, the enrichment in Cr and the correlation between V and Cr may be ascribed to the sole redox conditions.

4.4. Grain size of the glauconites of the sample set 2 (Assises de Croï Fm)

As mentioned in previous works, the HCl-leached fraction of the rock samples contains quasi-exclusively quartz and glauconite (Tribovillard et al., 2023a, 2023b). These two mineral species were efficiently separated using a magnetic separator and could be analyzed separately. The grain size analyzes are presented and discussed in Tribovillard et al. (2023b). The glauconite grains of the alternating carbonate and marly beds of the Assises de Croï Fm have been reported to have grown during earliest diagenesis, prior to the diagenetic precipitation of the carbonate beds (Tribovillard et al., 2023b). The results of importance for the present paper are gathered in Fig. 12 showing curves of grain size distribution for quartz and glauconite, whether they come from carbonate beds or from marly ones in the Assises de Croï Fm. The populations of quartz grains show a well-sorted, unimodal size distribution,

whereas the populations of glauconite grains are poorly sorted. The size distribution curves of the populations of quartz grains yield peaks between 100 μm and 200 μm for both bed and interbed facies. In contrast, the modes of the glauconite curves correspond to larger particle size in the marly beds compared to the carbonate beds. For the bed-hosted glauconites, all the curves but one are superimposed, with a main mode centered around 25 μm , whereas the curves of the interbed-hosted glauconites show modes dispersed between 30 μm and 100 μm . Thus, the glauconite particles of the marly beds are larger and more heterogeneous than those of the carbonate bed (they do not overlap so well). In contrast, the size distribution curves of the populations of quartz grains show similar patterns for the carbonate vs. marly beds, thus indicating that the level of hydrodynamic energy was similar for both environments of deposition. Thus, the discrepancy in the distribution of the glauconite grain sizes

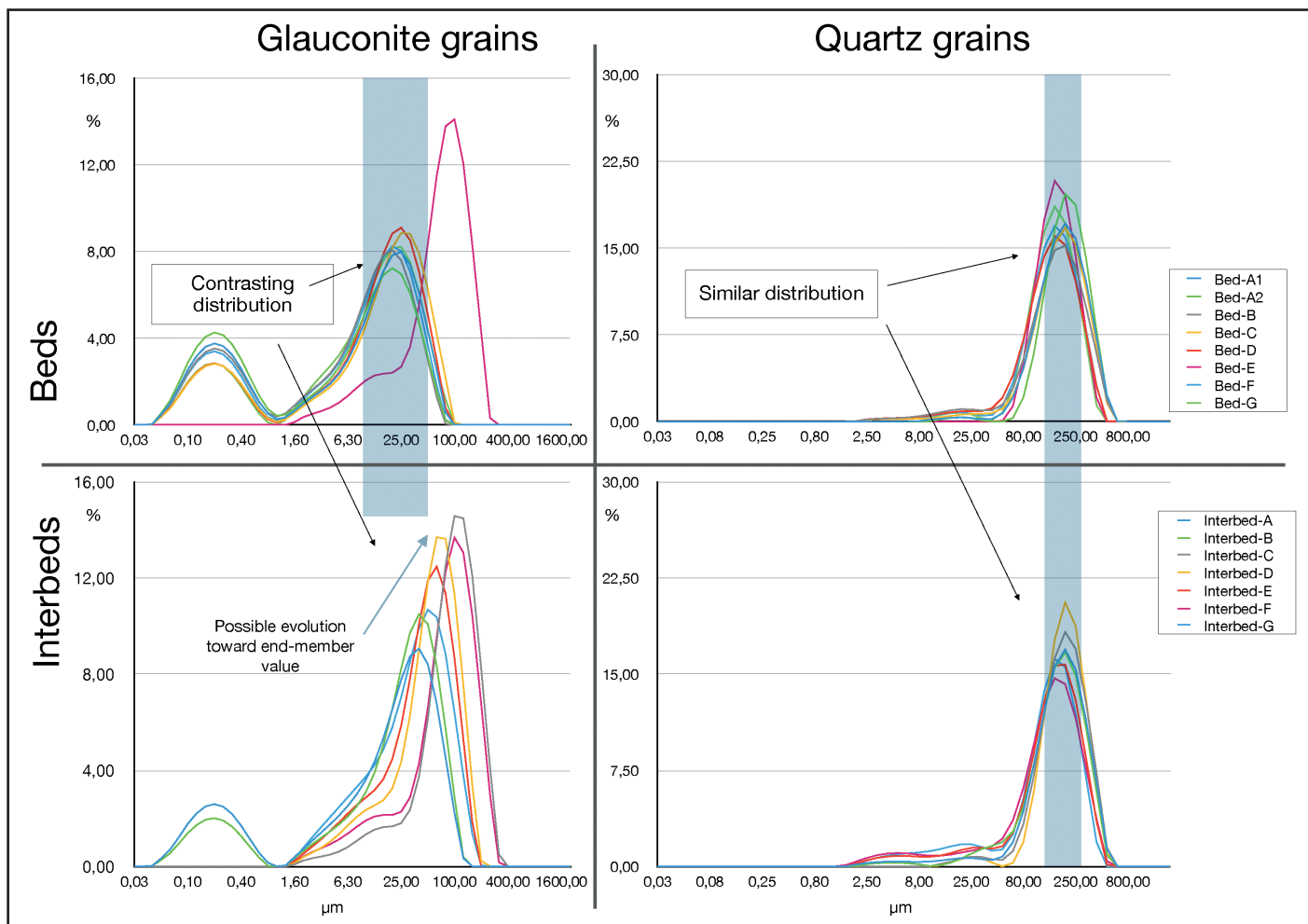


Fig. 12. Grain size distribution curves of glauconite and quartz grains from carbonate beds or marlstone beds of the Assises de Croï Fm. For the glauconite grains, the curves are superimposed in the carbonate beds (shaded area) but not in the marly ones. In the latter, the peaks tend toward an end-member position that can also be observed for the beds. For the quartz grains, the curves are similar for the beds and internats (shaded area).
 Fig. 12. Courbes de distribution granulométrique des grains de glauconite et de quartz des niveaux carbonatés ou marneux des Assises de Croï Fm. Pour les grains de glauconite, les courbes se superposent dans les lits carbonatés (zone grisée) mais pas dans les interbanes marneux. Dans ces derniers, les pics tendent vers une position extrême que l'on peut également observer pour les bancs calcaires. Pour les grains de quartz, les courbes sont similaires pour les bancs et les interbanes (zone ombrée).

cannot be explained by contrasted hydrodynamics but it can be accounted for by contrasted duration of authigenic growth. The glauconite in the case of marly beds is larger and more homogeneous in size, as if a prolonged growth of the authigenic grains would have tended towards a maximum terminal size over time (a sort of end member). At the end of the growth process, the authigenic grains would fall into a relatively narrow range of particle size value. Contrarily, inside the carbonate beds, the glauconite is smaller and less homogeneous in size. Glauconite growth preceded that of the carbonate beds, but the precipitation of carbonates isolated the glauconite grains from the marine environment as they were growing. Being isolated from their aqueous environment, the grains could not continue their growth and did not reach the same size limit as in the case of the grains of the marly beds, i.e., the size of syngenetic glauconites would reflect the duration of their growth. This hypothesis is supported by the geochemical argument discussed above: the glauconites of the depositional milieu characterized by low sedimentation rates are the richest in REE (highest Σ REE).

4.5. Implications for the causes of the limestone-marl alternation of the Assises de Croÿ Fm

The two facies of this formation are strikingly contrasted upon field observation; however, they cannot be distinguished using geochemical criteria (trace metals and REE) for glauconite examination. In other words, the glauconite witnessed what was going on during earliest diagenesis but did not record any difference or variation in the redox status of the sediment-water interface. This observation is in contrast with what Bellanca et al. (1997) observed, examining the bulk-rock REE distribution in limestone-marlstone couplets from the hemipelagic Cretaceous of Venetia. These authors carried out the sole study available in the literature (to the best of our knowledge; see also a related study by Su et al., 2020), comparing REE distribution in limestone beds vs. marly beds from limestone-marl alternations. They concluded that REE were impacted by redox conditions but they did not study specifically the authigenic phyllosilicate fractions. Their results encompass what was occurring in the entire water column and not specifically what was going on at the very sediment-water interface as is done in the present work.

The grain size distributions of quartz populations of both facies do not yield any difference, indicating that the levels of energy were similar during particle settling. Consequently, the diagenetic precipitation of limestone nodules and beds, which happened after sediment accumulation and glauconite growth, was not conditioned by the grain size of the detrital supply nor by redox conditions. The carbonate fraction of the beds bears the imprint of organic carbon in that the stable isotope composition of C shows negative values, differing from seawater signature of Late Jurassic seas and oceans (Tribovillard et al., 2023b). The nodules and beds growth

incorporated “light” carbon released by organic-matter remineralization, circulating per ascensum. Why the carbonate precipitation happened at specific levels within the sediments, forming continuous beds, is not evident. Nevertheless, it was not induced by the grain size distribution of the clastic particles. The role of permeability barriers opposing to fluid circulation and inducing carbonate saturation and precipitation can thus be ruled out. The carbonate supersaturation must be related to the presence of organic matter or methane, and biogenic bicarbonate ions inducing/fostering diagenetic precipitation, ending with limestone beds being aligned parallel to the sea bottom and bedding. See for instance the recent paper of Akam et al. (2023) and references therein. Such a stratal layout of authigenic carbonate beds and coalescent nodules was examined with the parallel two (occasionally three) beds of the Tithonian Bancs Jumeaux Fm of the Boulonnais (Table 1; Tribovillard et al., 2012). The explanations involved episodic spills of fluids onto the sea bottom, released by cold seepage sites. Our data do not allow this scenario to be ascertained in the present case but (at least some) alternative scenarios can be ruled out.

5. CONCLUSIONS

This work brings new elements to our understanding the complex mineral glauconite. First, the glauconites studied here show morphological and geochemical indications of maturity, according to the classical criteria, which suggests a protracted period of growth. Besides, over a range of age spanning the Late Jurassic and mid- and Late Cretaceous, and over a range of shelfal environments, the glauconite studied all show narrowly identical values for the Rb:K₂O and Sm:Nd ratios, respectively. Such constant ratios also suggest that a crystal chemical equilibrium had enough time to establish a balance, and that the authigenic growth was operating in an infinite reservoir, that is, close to the sediment-water interface. Long time, proximity to the sediment-water interface: both facts suggest slow sedimentation rates. However, in other respects, the glauconite grains of the Assises de Croÿ Fm terminated their growth during early diagenesis. Thus, it is concluded that glauconite can gain the signs of mineralogical maturity during early diagenesis. Early diagenesis is not incompatible with long time; nevertheless, all the glauconites at stake here formed in shelfal environments, that is, in places where sedimentation rates may hardly be close to zero during protracted periods of time. Intermittent sedimentation over time with repeated episodes of winnowing may explain a (relatively) long time for the formation of glauconite on the one hand, and an agitated sedimentary environment with terrigenous inputs, on the other hand. Anyway, as we have no means to assess the quantitative duration of the growth of glauconite, we will only refer to early diagenesis, regardless to its duration. Second, no robust information could be

derived from the REE distributions but one: the total amount of REE (Σ REE) could echo the duration of formation of glauconite. Therefore, our results reinforce the view that REE of authigenic minerals are of little help to decipher (past) environmental conditions of shallow marine milieus. Third, the limestone-marl alternation of the Assises de Croix Fm allows early diagenetic glauconite to be used as a witness of the conditions developing at or below the sediment-water interface. The facies alternation has no relation to see with alternating redox conditions affecting the sediment-water interface, nor with the hydrodynamic energy during particle settling. The reason(s) why diagenetic carbonate beds did form with a stratiform geometry remain a bit unclear but, at least, our results allow excluding some of the potential factors. Lastly, the grain size distribution of the glauconite grain populations is by far the clearest parameter allowing glauconite to be distinguished between diagenetic carbonate beds and marly interbeds. This study illustrates that the glauconite growth was hampered by the diagenetic formation of the carbonate beds that caged glauconite grains, thus preventing any further growth. Oppositely, glauconite growth was not hampered in the marly interbeds and the grains tended to an end-member size that could not be exceeded.

Acknowledgements. Our thanks go to the Programme Tellus Syster of the French Institut des Sciences de l'Univers (INSU) for funding our work. We thank Monique Gentric for the financial/administrative management, and Marion Delattre & Sandra Ventalon for the technical support of this project, as well as the LOG laboratory and the Department of Earth Sciences of the University of Lille for their support. This paper has been improved thanks to the reviews carried out by Jean-François Deconinck and François Guillot.

References

- AKAM S.A., SWANNER E.D., YAO H., HONG W.-L. & PECKMANN J. (2023). - Methane-derived authigenic carbonates – A case for a globally relevant marine carbonate factory. *Earth-Science Reviews*, **243**, 104487. <https://doi.org/10.1016/j.earscirev.2023.104487>.
- AMÉDRO F. & ROBASYNSKI F. (1999). - The Cenomanian chalk of the Boulonnais. Comparison with the Aube (France) and Kent (United Kingdom). *Géologie de la France*, **2**, 33-53.
- AMOROSI A. & CENTINEO M.C. (2000). - Anatomy of a Condensed Section: The Lower Cenomanian Glaucony-Rich Deposits of Cap Blanc-Nez (Boulonnais, Northern France). in Editor: C.R. Glenn, L. Prevot-Lucas, J. Lucas, *Marine Authigenesis: From Global to Microbial*, SEPM Society for Sedimentary Geology,
- BALDERMANN A., WARR L.N., GRATHOFF G.H. & DIETZEL M. (2013). - The rate and mechanism of deep-sea glauconite formation at the Ivory Coast – Ghana Marginal Ridge. *Clays and Clay Minerals*, **61**, 258–276. <https://doi.org/10.1346/CCMN.2013.0610307>.
- BALDERMANN A., BANERJEE S., CZUPPON G., DIETZEL M., FARKAŠ J., LÖHR S., MOSER U., SCHEIBLHOFFER E., WRIGH N.M. & ZACK T. (2022). - Impact of green clay authigenesis on element sequestration in marine settings. *Nature Communication*, **13**, 1527. <https://doi.org/10.1038/s41467-022-29223-6>
- BANERJEE S., BANSAL U., PANDE K. & MEENA S.S. (2016a). - Compositional variability of glauconites within the Upper Cretaceous Karai Shale Formation, Cauvery Basin, India: Implications for evaluation of stratigraphic condensation. *Sedimentary Geology*, **331**, 12-29.
- BANERJEE S., BANSAL U. & THORAT U.V. (2016b). - A review on palaeogeographic implications and temporal variation in glaucony composition. *Journal of Palaeogeography*, **5**, 43-71.
- BANERJEE S., CHATTORAJ S.L., SARASWATI P.K., DASGUPTA S. & SARKAR U. (2012a). - Mineralogy and geochemistry of lagoonal glauconites and their implications on origin and maturation: Oligocene Maniyara Fort Formation, western Kutch, India. *Geological Journal*, **47**, 357-371.
- BANERJEE S., CHATTORAJ S.L., SARASWATI P.K., DASGUPTA S. & SARKAR U. (2012b). - Substrate control on formation and maturation of glauconites in the Middle Eocene Harudi Formation, western Kutch, India. *Marine and Petroleum Geology*, **30**, 144-160. doi.org/10.1016/j.marpetgeo.2011.10.008.
- BANERJEE S., FAROUK S., NAGM E., ROY CHOUDHURY T. & MEENA S.S. (2019). - High Mg-glauconite in the Campanian Duwi Formation of Abu Tartur Plateau, Egypt and its implications. *Journal of African Earth Sciences*, **156**, 12-25. <https://doi.org/10.1016/j.jafrearsci.2019.05.001>.
- BANSAL U., BANERJEE S., PANDE K. & RUIDAS D.K. (2020). - Unusual seawater composition of the Late Cretaceous Tethys imprinted in glauconite of Narmada basin, central India. *Geological Magazine*, **137**, 233-247
- BANSAL U., SUNDAR RAJU P.V. & BANERJEE S. (2022). - Compositional evolution of glauconite within Proterozoic Gandikonta Formation, Cuddapah Basin, India and its implication. 21st International Sedimentological Congress, Beijing, T10-90412.
- BELLANCA A., MASETTI D. & NERI R. (1997). - Rare earth elements in limestone/marlstone couplets from the Albian-Cenomanian Cismon section (Venetian region, northern Italy): Assessing REE sensitivity to environmental changes. *Chemical Geology*, **141**, 141-152, DOI: 10.1016/S0009-2541(97)00058-2
- BREIT G.N. & WANTY R.B. (1991). - Vanadium accumulation in carbonaceous rocks : a review of geochemical controls during deposition and diagenesis. *Chemical Geology*, **91**, 83–97.
- BRUGGMANN S., SEVERMANN S. & MCMANUS J. (2023). - Geochemical conditions regulating chromium preservation in marine sediments, *Geochimica et Cosmochimica Acta*, **348**, 239-257, doi.org/10.1016/j.gca.2023.03.003.

- CARIGNAN J., HILD P., MOREL J. & YEGHICHEYAN D. (2004). - Routine analysis of trace elements in geochemical samples using flow injection and low-pressure on-line liquid chromatography coupled to ICP-MS: a study of geochemical reference materials BR, DR-N, UB-N, AN-G and GH. *Geostandard Newsletters*, **25**, 187–198.
- CHAFETZ H.S. & REID A. (2000). - Syndepositional shallow-water precipitation of glauconitic minerals. *Sedimentary Geology*, **136**, 29–42. [https://doi.org/10.1016/S0037-0738\(00\)00082-8](https://doi.org/10.1016/S0037-0738(00)00082-8)
- COLPAERT C.P.A.M., NIKITENKO B., DANELIAN T., FURSENKO H. & KOSENKO I. (2021). - Upper Kimmeridgian to Lower Tithonian foraminifers and ostracods of the Boulonnais region, Northern France. Stratigraphic and palaeoenvironmental implications and inter-regional correlations with the Siberian arctic. *Marine Micropaleontology*, **164**, 101976. <https://doi.org/10.1016/j.mar-micro.2021.101976>.
- DECONINCK J.-F., GEYSSANT J.R., PROUST J.-N. & VIDIER J.-P. (1996). - Sédimentologie et biostratigraphie des dépôts kimméridgiens du Boulonnais. *Annales de la Société Géologique du Nord*, **3** (2^e série), 157 - 170.
- DECONINCK J.-F. & BAUDIN F. (2008). - Kimmeridgian and Tithonian sedimentary deposits of the NorthWestern part of the Paris Basin (Normandy and Boulonnais). *Annales de la Société Géologique du Nord*, **15** (2^e série), 77–90.
- DENG Y., REN J., GUO Q., CAO J., WANG H. & LIU C. (2017). - Rare earth element geochemistry characteristics of seawater and porewater from deep sea in western Pacific. *Scientific Reports*, **7**, 16539. <https://doi.org/10.1038/s41598-017-16379-1>
- EL ALBANI A., MEUNIER A. & FURSICH F. (2005). - Unusual occurrence of glauconite in a shallow lagoonal environment (Lower Cretaceous, northern Aquitaine Basin, SW France). *Terra Nova*, **17**, 537–544.
- FLEET A.J., BUCKLEY H.A. & JOHNSON L.R. (1980). - The rare earth element geochemistry of glauconites and celadonites, *Journal of the Geological Society*, **137**, 683–688. <https://doi.org/10.1144/gsjgs.137.6.0683>
- FÖLLMI K.B. (2016). - Sedimentary condensation. *Earth-Science Reviews*, **152**, 143–180. <https://doi.org/10.1016/j.ear-scirev.2015.11.016>.
- GEYSSANT J.R., VIDIER J.-P., HERBIN J.-P., PROUST J.-N. & DECONINCK J.-F. (1993). - Biostratigraphie et paléoenvironnement des couches de passage Kimméridgien/Tithonien du Boulonnais (Pas de Calais): nouvelles données paléontologiques (ammonites) organisation séquentielle et contenu en matière organique. *Géologie de la France*, **4**, 11–24.
- GIRESE P. (2022). - Quaternary Glauconitization on Gulf of Guinea, Glauconite Factory: Overview of and New Data on Tropical Atlantic Continental Shelves and Deep Slopes. *Minerals*, **12**, 908. <https://doi.org/10.3390/min12070908>
- GIRESE P. & WIEWIÓRA A. (2001). - Stratigraphic condensed deposition and diagenetic evolution of green clay minerals in deep water sediments on the Ivory Coast–Ghana Ridge. *Marine Geology*, **179**, 51–70. [https://doi.org/10.1016/S0025-3227\(01\)00193-1](https://doi.org/10.1016/S0025-3227(01)00193-1)
- GIRESE P., BAYON G., TALLOBRE C. & LONCKE L. (2021). - Neodymium isotopes in glauconite for palaeoceanographic reconstructions at continental margins: a preliminary investigation from Demerara Rise. *Frontiers in Earth Sciences, Geochemistry*, **9**, 652501. <https://doi.org/10.3389/feart.2021.652501>
- GUSTAFSSON J.P. (2019). - Vanadium geochemistry in the biosphere – speciation, solid-solution interactions, and ecotoxicity. *Applied Geochemistry*, **102**, 1–25. <https://doi.org/10.1016/j.apgeochem.2018.12.027>
- HAASE F. J., VESSEY C. J., SEKINE R., DORIEAN N. J. C., WELSH D. T., OTTE J. A., HAMILTON J., CANFIELD D. E., WANG Y., LOMBI E. & BENNETT W. W. (2024). - Reductive sorption of vanadium by iron monosulfide in seawater. *Chemical Geology*, **649**, 121983. <https://doi.org/10.1016/j.chemgeo.2024.121983>
- HATEM E., TRIBOVILLARD N., AVERBUCH O., SANSJOFRE P., ADATTE T., GUILLOT F., ADER M. & VIDIER D. (2016). - Early diagenetic formation of carbonates in a clastic-dominated ramp environment impacted by synsedimentary faulting-induced fluid seepage – Evidence from the Late Jurassic Boulonnais Basin (N France). *Marine and Petroleum Geology*, **72**, 12–29. <https://doi.org/10.1016/j.marpetgeo.2016.01.010>.
- HUANG J.H., HUANG F., EVANS L. & GLASAUER S. (2015). - Vanadium: Global (bio) geochemistry. *Chemical Geology*, **417**, 68–89.
- HUGGETT J.M. (2021). Glauconites. in: *Encyclopedia of Geology* (Second Edition), pp. 334–340.
- HUGGETT J., ADETUNJI J., LONGSTAFFE F. & WRAY D. (2017). Mineralogical and geochemical characterisation of warm-water, shallow-marine glaucony from the Tertiary of the London Basin. *Clay Minerals*, **52**, 25–50. [doi:10.1180/claymin.2017.052.1.02](https://doi.org/10.1180/claymin.2017.052.1.02)
- JARRAR G., AMIREH B. & ZACHMANN D. (2000). - The major, trace and rare earth element geochemistry of glauconite from the early Cretaceous Kurnub Group of Jordan. *Geochemical Journal*, **34**, 207–222. DOI: 10.2343/geochemj.34.207
- KECHICHED R., LAOUAR R., BRUGUIER O., SALMI-LAOUAR S., KOCSIS L., BOSCH D., FOUFOU A., AMEUR-ZAIMECHE O. & LARIT H. (2018). - Glauconite-bearing sedimentary phosphorites from the Tébessa region (eastern Algeria): Evidence of REE enrichment and geochemical constraints on their origin. *Journal of African Earth Sciences*, **145**, 190–200. <https://doi.org/10.1016/j.jafrearsci.2018.05.018>.
- LÓPEZ-QUIRÓS A., ESCUTIA C., SÁNCHEZ-NAVAS A., NIETO F., GARCIA-CASCO A., MARTÍN-ALGARRA A., EVANGELINOS D. & SALABARNADA A. (2019). - Glaucony authigenesis, maturity and alteration in the Weddell Sea: An indicator of paleoenvironmental conditions before the onset of Antarctic glaciation. *Sci. Rep.* **9**, 13580. <https://doi.org/10.1038/s41598-019-50107-1>
- MEUNIER J.D., (1994). - The Composition and Origin of Vanadium-Rich Clay Minerals in Colorado Plateau Jurassic Sandstones. *Clay Clay Miner.* **42**, 391–401.



- MEUNIER A. & EL ALBANI A. (2007). - The glauconite–Fe-illite–Fe-smectite problem: a critical review. *Terra Nova*, **19**, 95-104.
- MORSE J.W. & MACKENZIE F.T. (1990). - Geochemistry of Sedimentary Carbonates. *Developments in sedimentology*, **48**, 707 p., Elsevier, Amsterdam.
- MURRAY R.W., BUCHHOLZ TEN BRINK M.R., JONES D.L., GERLACH D.C. & RUSS III G.P. (1990). - Rare earth elements as indicators of different marine depositional environments in chert and shale. *Geology*, **18**, 268-271. [https://doi.org/10.1130/0091-7613\(1990\)018<0268:REEAIO>2.3.CO;2](https://doi.org/10.1130/0091-7613(1990)018<0268:REEAIO>2.3.CO;2)
- ODIN G.S. & MATTER A. (1981). - De glauconiarum origine. *Sedimentology*, **28**, 611–641.
- ODIN G.S. (1988). - Chapter C1 Glaucony from the Gulf of Guinea, Editor(s): G.S. Odin, *Developments in Sedimentology*, Elsevier, Volume 45, 225-247. [https://doi.org/10.1016/S0070-4571\(08\)70066-9](https://doi.org/10.1016/S0070-4571(08)70066-9).
- OLU K, DUPERRET A., SIBUET M., FOUCHER J.-P. & FIALA-MEDIONI A. (1996). - Structure and distribution of cold seep communities along the Peruvian active margin: relationship to geological and fluid patterns. *Marine Ecology Progress Series*, **132**, 109-125.
- OZE C., SMAILL J.B., REID C.M. & PALIN M. (2019). - Potassium and metal release related to glaucony dissolution in doils. *Soil Systems*, **3**, 70. <https://doi.org/10.3390/soilsystems3040070>
- PIPER D.Z. (1974). - Rare earth elements in the sedimentary cycle: A summary. *Chemical Geology*, **14**, 285-304. [https://doi.org/10.1016/0009-2541\(74\)90066-7](https://doi.org/10.1016/0009-2541(74)90066-7)
- RAFIEI M., LÖHR S., ALARD O., BALDERMANN A., FARKAŠ J. & BROCK G. (2023). - Microscale petrographic, trace element, and isotopic constraints on glauconite diagenesis in altered sedimentary sequences: implications for glauconite geochronology. *Geochemistry, Geophysics, Geosystems*, **24**, e2022GC010795, 1-24. <https://doi.org/10.1029/2022GC010795>,
- ROLLINSON H. & PEASE V. (2021). - *Using Geochemical Data: To Understand Geological Processes* (2nd ed.). Cambridge: Cambridge University Press. doi:10.1017/9781108777834
- ROUXEL O.J., GALY A. & ELDERFIELD H. (2006). - Germanium isotopic variations in igneous rocks and marine sediments. *Geochimica et Cosmochimica Acta*, **70**, 3387-3400, <https://doi.org/10.1016/j.gca.2006.04.025>
- ROY CHOUDHURY T., BANERJEE S., KHANOLKAR S. & MEENA S.S. (2021a). - Paleoenvironmental conditions during the Paleocene-Eocene transition imprinted within the glauconitic Giral Member of the Barmer Basin, India. *Minerals* **12**, <https://doi.org/10.3390/min12010056>
- ROY CHOUDHURY T.R., BANERJEE S., KHANOLKAR S., SARASWATI P.K. & MEENA S.S. (2021b). - Glauconite authigenesis during the onset of the Paleocene-Eocene thermal Maximum: a case study from the Khuiala Formation in Jaisalmer Basin, India. *Palaeogeography, Palaeoclimatology, Palaeoecology*, **571**, 110388. <https://doi.org/10.1016/j.palaeo.2021.110388>
- ROY CHOUDHURY T., SINGH P., CHAKRABORTY A. & BANERJEE S. (2023). - Authigenic Fe mineralization in shallow to marginal marine environments: a case study from the Late Paleocene–Early Eocene Cambay Shale Formation. *Minerals*, **13**, 646. <https://doi.org/10.3390/min13050646>
- SEMENIUK D.M., MALDONADO M.T. & JACCARD S.L. (2016). - Chromium uptake and adsorption in marine phytoplankton – Implications for the marine chromium cycle. *Geochimica et Cosmochimica Acta*, **184**, 41-54. <https://doi.org/10.1016/j.gca.2016.04.021>.
- SHOLKOVITZ E.R. & SCHNEIDER D.L. (1991). - Cerium redox cycles and rare earth elements in the Sargasso Sea. *Geochimica et Cosmochimica Acta*, **55**, 2737-2743. [https://doi.org/10.1016/0016-7037\(91\)90440-G](https://doi.org/10.1016/0016-7037(91)90440-G)
- SINGH P., BANERJEE S., ROY CHOUDHURY T., BHATTACHARYA S. & PANDE K. (2023). - Distinguishing celadonite from glauconite for environmental interpretations: a review. *Journal of Palaeogeography*, **12**, 179-194, <https://doi.org/10.1016/j.jop.2023.02.001>.
- STILLE P. & CLAUER N. (1994). - The process of glauconitization: chemical and isotopic evidence. *Contributions in Mineralogy and Petrology*, **117**, 253–262. <https://doi.org/10.1007/BF00310867>
- SU C., LI F., TAN X., GONG Q., ZENG K., TANG H., LI M. & WANG X. (2020). - Recognition of diagenetic contribution to the formation of limestone-marl alternations: A case study from Permian of South China. *Marine and Petroleum Geology*, **111**, 765-785. <https://doi.org/10.1016/j.marpetgeo.2019.08.033>.
- SUESS E. (2014). - Marine cold seeps and their manifestations: geological control, biogeochemical criteria and environmental conditions. *International Journal of Earth Sciences*, **103**, 1889–1916. <https://doi.org/10.1007/s00531-014-1010-0>
- TALLOBRE C., GIRESSE P., BASSETTI M.-A., LONCKE L., BAYON G., BUSCAIL R., TUDRYN A. & ZARAGOSI S. (2019). - Formation and evolution of glauconite in the Demerara Contourite depositional system related to NADW circulation changes during late Quaternary (French Guiana). *Journal of South American Earth Sciences*, **92**, 167-183, <https://doi.org/10.1016/j.jsames.2019.03.011>.
- TAYLOR S.R., MCLENNAN, S.M. (1985). - *The Continental Crust: Its Composition and Evolution*. Blackwell, Oxford.
- TOSTEVIN R., SHIELDS G.A., TARBUCK G.M., HE T., CLARKSON M.O. & WOOD R.A. (2016). - Effective use of cerium anomalies as a redox proxy in carbonate-dominated marine settings. *Chemical Geology*, **438**, 146-162. <https://doi.org/10.1016/j.chemgeo.2016.06.027>.
- TRIBOVILLARD N. (2013). - The Ge/Si ratio as a tool to recognize biogenic silica in chert. *Comptes Rendus Geoscience*, **345**, 160–165.
- TRIBOVILLARD N., ALGEO T.J., LYONS T. & RIBOULLEAU A. (2006). - Trace metals as paleoredox and paleoproductivity proxies: an update. *Chemical Geology*, **232**, 12–32.
- TRIBOVILLARD N., BOUT-ROUMAZEILLES V., RIBOULLEAU A., BAUDIN F., DANELIAN T. & RIQUIER L. (2011). - Transfer of germanium to marine sediments: insights from its accumu-

- lation in radiolarites and authigenic capture under reducing conditions. Some examples through geological ages. *Chemical Geology*, **282**, 120–130.
- TRIBOVILLARD N., SANSJOFRE P., ADER M., TRENTESAUX A., AVERBUCH O. & BARBECOT F. (2012). - Early diagenetic carbonate bed formation at the sediment-water interface triggered by synsedimentary faults. *Chemical Geology*, **300/301**, 1–13.
- TRIBOVILLARD N., BOUT-ROUMAZEILLES V., DELATTRE M., VENTALON S., ABRAHAM R. & NZIÉ O. (2021). - Syndepositional glauconite as a paleoenvironmental proxy - the lower Cenomanian Chalk of Cap Blanc Nez (N-France). *Chemical Geology*, **584**, 120508, doi.org/10.1016/j.chemgeo.2021.120508.
- TRIBOVILLARD N., BOUT-ROUMAZEILLES V., ABRAHAM R., VENTALON S., DELATTRE M. & BAUDIN. F. (2023a). - The contrasting origins of glauconite in the shallow marine environment highlight this mineral as a marker of paleoenvironmental conditions. *Comptes Rendus. Geoscience*, **355**, 213-228. https://doi.org/10.5802/crgeos.170
- TRIBOVILLARD N., BOUT-ROUMAZEILLES V., GUILLOT F., BAUDIN F., DECONINCK J.-F., ABRAHAM R. & VENTALON S. (2023b). - A sedimentological oxymoron: highly evolved glauconite of earliest diagenetic origin. *Comptes Rendus Geoscience*, **355**, 157-173. https://doi.org/10.5802/crgeos.
- TUTTLE M.L.W., BREIT G.N. & GOLDBERGER M.B. (2009). - Weathering of the New Albany Shale, Kentucky: II. Redistribution of minor and trace elements. *Applied Geochemistry*, **24**, 1565-1578. https://doi.org/10.1016/j.apgeochem.2009.04.034.
- VAN HOUTEN F.B. & PURUCKER M.E. (1985). - On the origin of glauconitic and chamositic granules. *Geo-Marine Letters*, **5**, 47-49. DOI: 10.1007/BF02629797
- VELDE B. (2014). - Sediments, Diagenesis and Sedimentary Rocks. in: *Treatise on Geochemistry* (Second Edition), Elsevier, Amsterdam, vol. **9**, pp. 351-36.
- WANG X., LI C. & ZHOU L. (2017). - Metal concentrations in the mussel *Bathymodiolus platifrons* from a cold seep in the South China Sea. *Deep Sea Research Part I: Oceanographic Research Papers*, **129**, 80-88. https://doi.org/10.1016/j.dsr.2017.10.004.
- WANTY R.B. & GOLDBERGER (1992). - Thermodynamics and kinetics of reactions involving vanadium in natural systems: accumulation of vanadium in sedimentary rock. *Geochimica et Cosmochimica Acta*, **56**, 1471–183.
- WIEWIORA A. & LACKA B. (1985). - Aspects de la minéralogénèse des glauconies. *Sciences Géologiques Bulletin*, **38**, 323-335.
- WIGLEY R. & COMPTON J.S. (2007). - Oligocene to Holocene glauconite–phosphorite grains from the Head of the Cape Canyon on the western margin of South Africa, *Deep Sea Research Part II: Topical Studies in Oceanography*, **54**, 1375-1395. https://doi.org/10.1016/j.dsr2.2007.04.004.
- WILDE P., QUINBY-HUNT M.S. & ERDTMANN B.D. (1996). - The whole-rock cerium anomaly: a potential indicator of eustatic sea-level changes in shales of the anoxic facies. *Sedimentary Geology*, **101**, 43-53. DOI: 10.1016/0037-0738(95)00020-8
- WILMSEN M. & BANSAL U. (2021). - Depositional setting and limiting factors of early Late Cretaceous glaucony formation: implications from Cenomanian glauconitic strata (Elbtal Group, Germany). *Facies* **67**(3), DOI: 10.1007/s10347-021-00627-y
- ZHANG K. & SHIELDS G.A. (2023). - Early diagenetic mobilization of rare earth elements and implications for the Ce anomaly as a redox proxy. *Chemical Geology*, **635**, 121619, doi.org/10.1016/j.chemgeo.2023.121619.
- ZHANG Q., WU D., JIN G., MAO S., LIU J., YANG C., LIU L., XU X., YANG P., CAO Y. & SU Z. (2022). - Novel use of unique minerals to reveal an intensified methane seep during the last glacial period in the South China Sea. *Marine Geology*, **452**, 10690. https://doi.org/10.1016/j.margeo.2022.106901.